HASP Student Payload Application for 2018

Payload Title: Stratospheric Spectropolarimeter Gamma-X (SSGX)	
Institution: American River College (USA), University of Coimbra (Portugal), INAF-IASF Bologna (Italy)	
Payload Class (Enter SMALL, or LARGE): LARGE	Submit Date: February 16, 2018

Project Abstract: Among the frontiers of astronomy are the polarization measurements of x- and γ-rays, emitted from phenomena such as γ-ray bursts, pulsars, and active galactic nuclei. Our payload utilizes a 4x4 pixel CdTe array developed to characterize background radiation in the 20-1000 keV energy range. SSGX features both the CACTμS detection unit (previously launched from Italy in 2002) and an innovative electronic data collection system designed by ARC students. DAISI samples detector analog voltages, supplies required voltages, monitors system operation, regulates electronics temperature, responds to remote communication, and continuously records acquired data as well as system status to permanent storage. Preparing for integration, the SSGX is contained within a (31 x 26 x 30) cm^3 volume, has a mass of 9.99 kg, utilizes a maximum current draw of 1.497 A, and communicates at an effective data rate of 70.4 bps. This relatively modest experiment is crucial for developing reliable calibration data for future instrumentation. Further, this project provisions international collaboration between ARC undergraduates and research partners in Portugal and Italy. Our goal is thus to obtain, for the first time, a fine measurement of all background components capable of deteriorating a γ-ray polarimeter response in space.

Team Name: ARC Physics and Astronomy Club		Team or Project Website: https://github.com/Sternzeug/DAISI
	Student Leader Contact Information:	Faculty Advisor Contact Information:
Name:	Stacey Burrows	Professor Paulo Afonso
Department:	Physics and Astronomy	Physics and Astronomy
Mailing Address:	American River College 4700 College Oak Drive	American River College 4700 College Oak Drive
City, State, Zip code:	Sacramento, CA 95841	Sacramento, CA 95841
e-mail:	stacey.a.burrows@gmail.com w1446026@apps.losrios.edu	afonsop@arc.losrios.edu
Office Telephone:	(916) 923-3665	(916) 484-8733
Mobile Telephone:	(916) 712-1878	(530) 574-1632

Table of Contents

I. Payload Description **3**
1.1 Scientific Background 3
1.2 Polarimetry Fundamentals and Simulation 4
1.2.1 Polarization Fundamentals 4
1.2.2 Polarization Simulations 6
1.3 Scientific Goals of Balloon Flight Experiment 7
1.3.1 Scientific Goals 7
1.3.2 Background Sources 8
1.3.3 Previous Flight Experience 10
1.4 Payload Systems and Flight Operation 14
1.4.1 Detection System 15
1.4.2 Payload Electronics 17
1.4.3 Firmware Design 20
1.4.4 Thermal Control 22
1.4.5 Anticipated Software Development 22

II. Team Structure & Management **23**
Table 1: Project Contributors 25
Table 2: Anticipated HASP 2018 Development Timeline 27

III. Payload Interface **29**
3.1 Payload Dimensions 29
3.2 Weight Distribution 31
Table 3: Weight Budget 31
3.3 HASP Integration Plan 31
Table 4: Platform Connections Pin-Out 35
3.4 Electrical Distribution 35
Table 5: Current Consumption 37
3.5 Communication Plan 38
Table 6: HASP Command String and Student Payload Command Format 38
Table 7: Status Update Record Format 39
Table 8: Current DAISI RS-232 Command List 40

IV. Preliminary Drawings **41**
4.1 Payload and Platform Integration 41
4.2 Power Circuit Diagrams 42
4.3 Additional Schematic Diagrams 44

I. Payload Description

1.1 Scientific Background

High-energy astrophysics polarimetry has experienced only modest exploration due to the high degree of complexity -- not only in detection methodology and the related electronic signaling and processing systems, but also due to the specific constraints in the targets of interest. Celestial γ-rays can only be observed from either space, sounding rockets, or via high-altitude balloon missions. To date, x- and γ-ray emissions have been studied almost exclusively through spectral and timing variability analysis, or by using imaging techniques based on coded mask cameras or telescopes equipped with high-efficiency focal plane detectors.

Comparatively, by measuring the polarization angle and degree of linear polarization of the detected emissions, the number of observational parameters is increased by two, thereby enhancing discrimination between different models that characterize the same object. Polarimetric observations can provide important information about the geometry, magnetic field, composition and emission mechanisms of astrophysical sources. Polarization and degree are typically independent parameters, providing geometric information about a specific object, which is decoupled from its physical processes; this enables improvements in modeling, independent of physical principles. Polarized x- and γ-ray emissions are expected from a wide variety of sources, including pulsars, solar flares, active galactic nuclei, galactic black holes, and γ-ray bursts [1].

Polarization in the x-ray (<10 keV) domain has been observed at least since the 1970s, as exemplified by the Aerobee-350 sounding rocket flight (from NASA's Wallops Island) and by OSO-8's (Orbiting Solar Observatory) polarimeter -- each of which measured the Crab Nebula polarization [2,3]. Progress in γ-ray astronomy has been more difficult to achieve. Although further space-dedicated polarimeters have been proposed [4-7], the first conclusive polarimetric measurements in the soft γ-ray domain (100 keV - 1 MeV) was performed by the INTEGRAL (INTErnational Gamma-Ray Astrophysics Laboratory) mission, launched in 2002 [8,9]. These observations of the Crab Pulsar and the stellar black hole Cygnus X-1 [10-12], were made using INTEGRAL's instruments SPI (Spectrometer on INTEGRAL) and IBIS (Imager on Board the INTEGRAL Satellite).

1.2 Polarimetry Fundamentals and Simulation

1.2.1 Polarization Fundamentals

The importance of polarimetry is today largely recognized within the high-energy astrophysical community, thus the next generation of space missions aims to provide polarimetric observations of the high-energy Universe. This is indeed the case for the high-energy (300 keV - 3 GeV) space mission proposal asserted by the e-ASTROGAM Consortium for the fifth medium-sized European Space Agency Cosmic Vision program (M5). Polarimetry is in fact among the main objectives for this mission proposal [13]. In the framework of the development of e-ASTROGAM's focal plane optimized for polarimetry (several detector types are being considered, such as Si and Ge), a CdTe polarimeter prototype was tested under a partially polarized beam generated by Compton scattering on a target, when irradiated by a ^{22}Na (511 keV) radioactive source.

The balloon experiment herein proposed represents a constituent element of a larger project that includes vast polarimetry simulations with GEANT4 and a series of experiments carried out at the ESRF (European Synchrotron Radiation Facility) under monochromatic-polarized beams between 100 and 750 keV [14-19]. In this energy band, polarimetry is based in Compton Scattering.

The polarimetric performance of a focal plane detector is determined by the fundamental concepts associated with polarized Compton interactions. The Compton scattering of polarized photons generates non-uniformity in the azimuthal angular distribution. After undergoing Compton scattering, the polarized photon's new direction depends on the orientation of its polarization before the interaction. If the polarized photon undergoes a new interaction inside the detector, the statistical distribution of the relative positions of the two interactions (double event) allows for inference of the degree and polarization direction of the incident radiation. The Klein-Nishina cross-section for linearly polarized photons gives us an azimuthal dependency for the scattered photons:

$$\frac{d\sigma}{d\Omega} = \frac{r_0^2}{2}\left(\frac{E'}{E}\right)^2\left[\frac{E'}{E} + \frac{E}{E'} - 2\sin^2\theta\cos^2\varphi\right] \quad (1)$$

Where $\mathbf{r_0}$ is the classical electron radius, **E** and **E'** are the energies of the incoming and outgoing photons (respectively), $\boldsymbol{\Theta}$ the angle of the scattered photon, and $\boldsymbol{\varphi}$ is the angle between the scattering plane (defined by the incoming and outgoing photon directions) and incident polarization plane (defined by the polarization direction and the direction of the incoming photon). As can be seen from (1), after fixing all other parameters the probability of interaction varies with the azimuthal angle $\boldsymbol{\varphi}$ and its maximum and minimum arises for orthogonal directions. For $\boldsymbol{\varphi}$= 0° the cross-section reaches a minimum and for $\boldsymbol{\varphi}$ = 90° the cross-section reaches a maximum. However, this relative difference is maximized for an angle $\boldsymbol{\Theta}_M$, dependent

on the incident photon energy. For soft γ- and hard X-rays (100 keV - 1 MeV) the Θ_M value is about 90°.

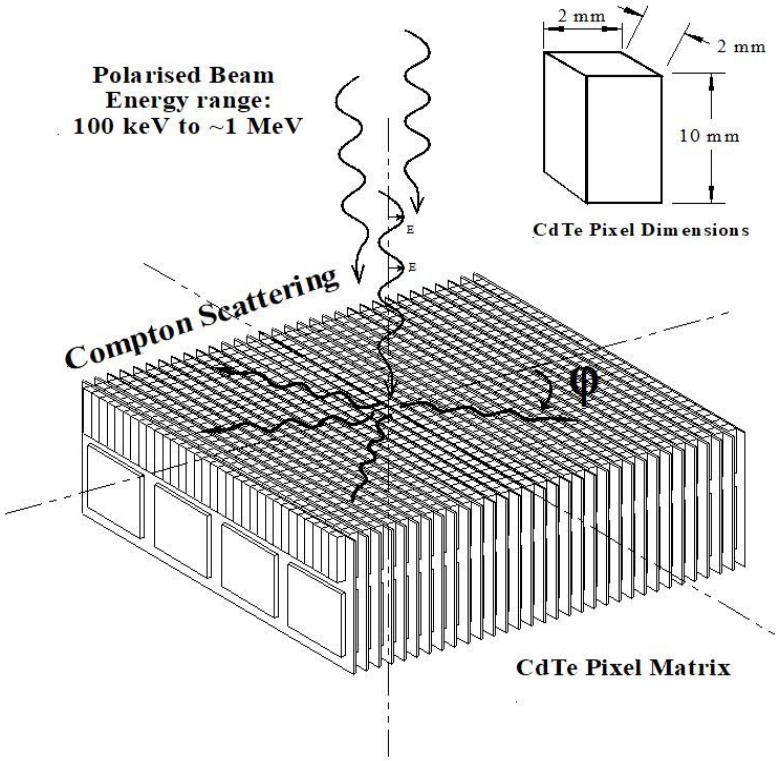

Fig. 1 - Compton scattering in a CdTe pixel matrix. Illustration taken from [14].

The polarimetric performance of an instrument can be evaluated by analyzing the distribution of double events through the polarimetric modulation factor, Q. This is obtained by integrating the Compton polarimetric differential cross-section formula given by (1) over the solid angles defined by the physical geometry of the detection plane, and for a pixel detector can be written as:

$$Q = \frac{N_x - N_y}{N_x + N_y} \qquad (2)$$

Here we obtain Q through the number of double events, N_x and N_y, integrated over two orthogonal directions (x and y) defined over the detector plane.

1.2.2 Polarization Simulations

In order to predict the CdTe polarimetric performance, researchers typically develop Monte Carlo codes based on GEANT4 library modules in order to simulate the detector behaviour under polarized and unpolarized photon fluxes. This is a prerequisite for ulterior comparison with flight data.

GEANT4, an acronym for GEometry ANd Tracking, is a software toolkit used for simulating the passage of particles through matter. Its areas of application include high energy, nuclear and accelerator physics, as well as studies in medical and space sciences.

Simulations typically focus on two main aspects: physical and geometric. The physical concepts involve electromagnetic interactions, particularly with respect to polarized Compton scattering. The detection geometry concepts focus on aspects such as beam characteristics, detection plane, and read-out geometry. A complete simulation must, therefore, include factors such as the energy of the beams, their inclination angles, efficiency of the detectors, etc..

Clarifying further the content of Fig. 1, the illustration below shows the scattering probability diagram from the Klein-Nishina (KN) equation (1) as a function of the azimuthal angle, **φ**. It also shows a generic Compton scattering event, where the incoming photon is represented in blue and the scattered photon is represented in red.

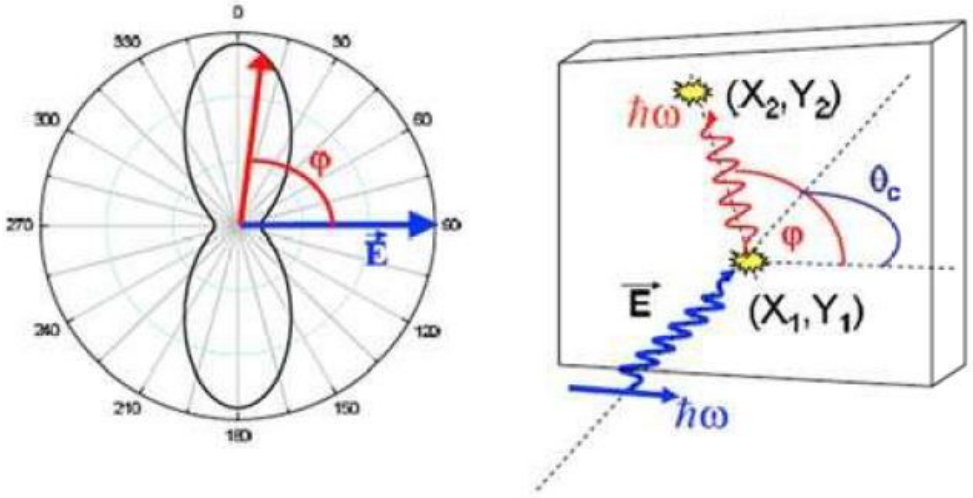

Fig. 2 - On the left, the scattering probability diagram from the KN equation. The electrical field vector E indicates the direction of the photons' polarization plane. On the right, a Compton scattering event, with a scattering angle (labeled $\boldsymbol{\Theta}_C$) of 90°. Illustration taken from [20].

Figure 3 below shows a specific simulation example of the theoretical distribution of double events in a CdTe pixel matrix. The generated model demonstrates a Compton scattering event in the central pixel, followed by a photoelectric absorption of the scattered photon in a peripheric pixel. In Figure 3a, the distribution exhibits an oblong shape produced from the simulation of a 100% linearly polarized beam at 200 keV, normal to the detector surface with a polarization angle of 30°. In this case, the main scattering axis distribution is perpendicular to the polarization vector. Figure 3b represents the same simulation, however with an unpolarized incident beam shown without a preferred scattering direction visible on the simulation map.

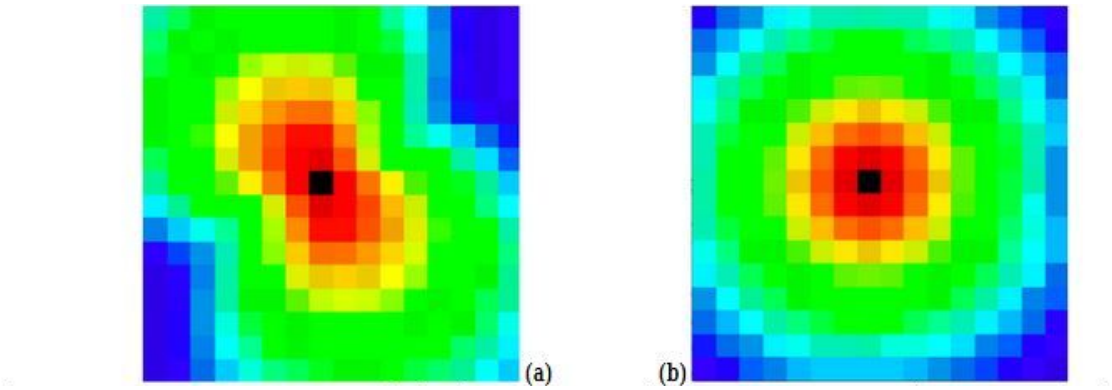

Fig. 3 (a) - 100% linearly polarized beam with an angle of polarization of 30°.
Fig. 3 (b) - Unpolarized photon beam.
Both images represent the numerical simulations of a 200 keV beam, where red indicates high probability and blue indicates lower probability. Images taken from [21].

1.3 Scientific Goals of Balloon Flight Experiment

1.3.1 Scientific Goals

Extensive polarimetric analysis with CdTe prototypes has been conducted, both by simulation and experimentally. A balloon experiment is highly suitable for further analysis of parameters critical to designing a γ-ray polarimeter for space applications. Since celestial-source polarimetric measurements are not likely achievable during a balloon flight due to very low γ-ray flux at balloon altitude combined with detector sensitivity limitations within a balloon payload, measuring the double events' background would be notably useful in determining the expected sensitivity of the instrument's space configuration.

Polarimetric sensitivity has a strong dependence on background noise, therefore measuring the double events produced by background radiation should provide critical information for further polarimeter development. Thus far, data is available exclusively for single events' background. By measuring the double events' background, as well as that of multiple events (photons

undergoing more than two interactions in different pixels), and incorporating this data with data for known single events, we would then be able to estimate all possible background components. Therefore, obtaining a far more precise background flux will allow for optimizations in future instrument design with respect to minimization of expected space background.

1.3.2 Background Sources

Since double events are generated by a celestial background of randomly polarized photons, it is important to discuss the expected corresponding sources. The fluxes of x- and γ-rays detected throughout Earth's atmosphere essentially result from galactic cosmic rays (GCR), solar flares, and even phenomena such as lightning and terrestrial γ-ray flashes (the latter of which was discovered in 1994, and is more prevalent at lower altitudes).

Radiation levels typically increase with altitude when exclusively considering the primary cosmic rays component. The Pfotzer maxima, however, result from the combination of the decreased density of primaries and increased density of particles created in secondary showers with increasing atmospheric depth.

Adding to this complexity, GCR levels in Earth's atmosphere further vary by latitude (due to geomagnetic effects) and relative to solar activity. Outside Earth's magnetic field, the composition of GCR is 98% protons, with the remaining 2% consisting of alpha particles, heavier nuclei, electrons, positrons, and even very high energy γ-rays (above 10^{16} eV).

The inner radiation belt starts at around 200 km above Earth's surface, consisting mostly of electrons and very high energy protons (10 – 100 MeV). Antimatter (another source of γ-rays) was first found in atmospheric cosmic rays in 1932. More recently, International Space Station-based discoveries revealed regions of the Van Allen belts with positrons' concentration levels higher than expected.

Above energies of 50 MeV, the main source of atmospheric gamma radiation background is the decay of mesons. Below 50 MeV (our region of interest) the dominant effect is *bremsstrahlung* (or "braking radiation") of secondary and reentrant albedo electrons, with a smaller contribution from primary cosmic ray electrons.

The physics of cosmic ray showers is complex and compelling, as illustrated in the general figure provided by CERN below. For instance, among many other reactions: on impacting a nucleus of nitrogen in the upper atmosphere, a neutron can induce emission of γ-rays by nuclear excitation. Alternately, it can break the nucleus, producing albedo neutrons that later decay into protons and electrons. These neutron nuclear reactions also produce neutral pions (among others) that decay into gamma photons.

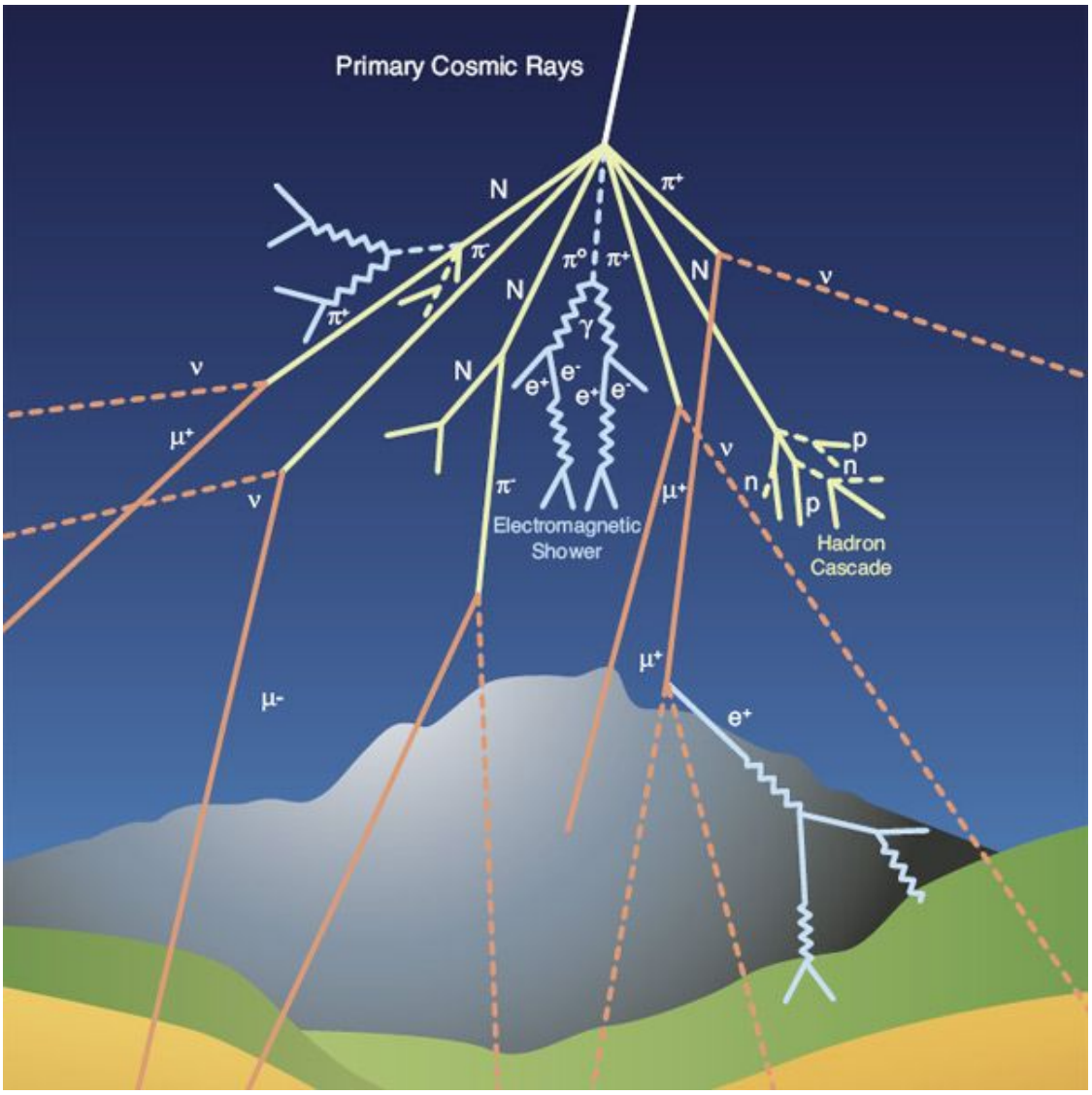

Fig. 4 - Cosmic rays' general interactions in the atmosphere are shown here, indicating the hadronic cascade and electromagnetic shower as part of the secondary cosmic rays. (CERN illustration)

Given the array of contributing factors, the number of background x- and γ-ray photons counted per second thus depends highly on the energy of the particular phenomenology involved. As illustrated in Figure 5 below, in addition to changing with energy, the counting rate also depends on the type of shielding utilized.

Integrating overall the energy values of interest, 10 000 counts/second is a typical upper limit used in GEANT detection simulations – even if expecting somehow lower fluxes in reality.

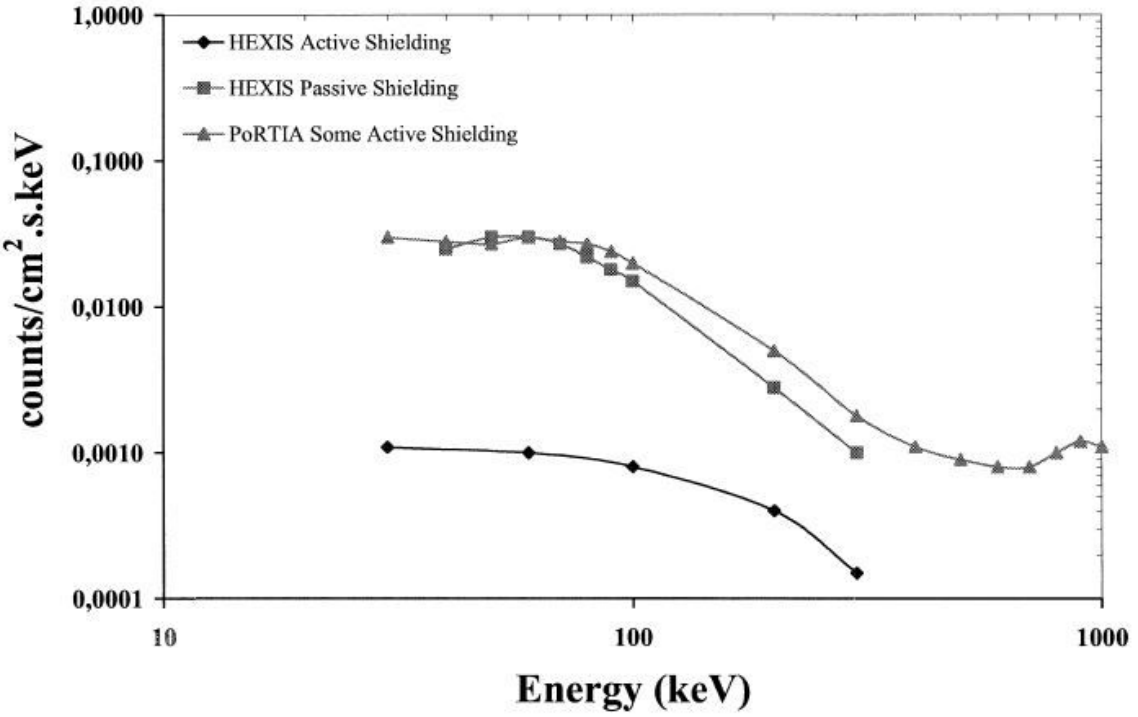

Fig. 5 - These two measurements of background levels were obtained in different stratospheric balloon experiments. The PoRTIA (Piggyback Room Temperature Instrument for Astronomy) on board the GRIS (Gamma-Ray Imaging Spectrometer) mission launched from Alice Springs (Australia, 1994); HEXIS (High Energy X-ray Imaging Spectrometer) launched from Palestine, Texas (USA, 2000). Both are based on CdZnTe detection elements with properties similar to our SSGX CdTe matrix, and thus both provide a suitable comparison. The data from the Alice Springs and Palestine flights were corrected according to the difference in geomagnetic latitudes.
Illustration taken from [14].

1.3.3 Previous Flight Experience

Our Stratospheric Spectropolarimeter Gamma-X (SSGX) payload is based on the detection capacities of the Compact Array of Cadmium Telluride Micro Spectrometers (CACTμS), [22]. The CACTμS detector launched from Sicily, Italy in 2002. During its twelve-hour flight, CACTμS collected data exclusively for single events' background. We now propose to explore the implementation of coincidence logic for the characterization of double and multiple events. Double events (two hits within different pixels, the first interaction being a Compton) are essential in determining Compton photons' new direction and therefore the polarization direction.

The CACTμS instrument includes the primary detector housing (CdTe detectors) with associated front-end electronics (voltage supplies, temperature sensors, Charge Sensitive Preamps/CSPs), shown below in Figure 6.

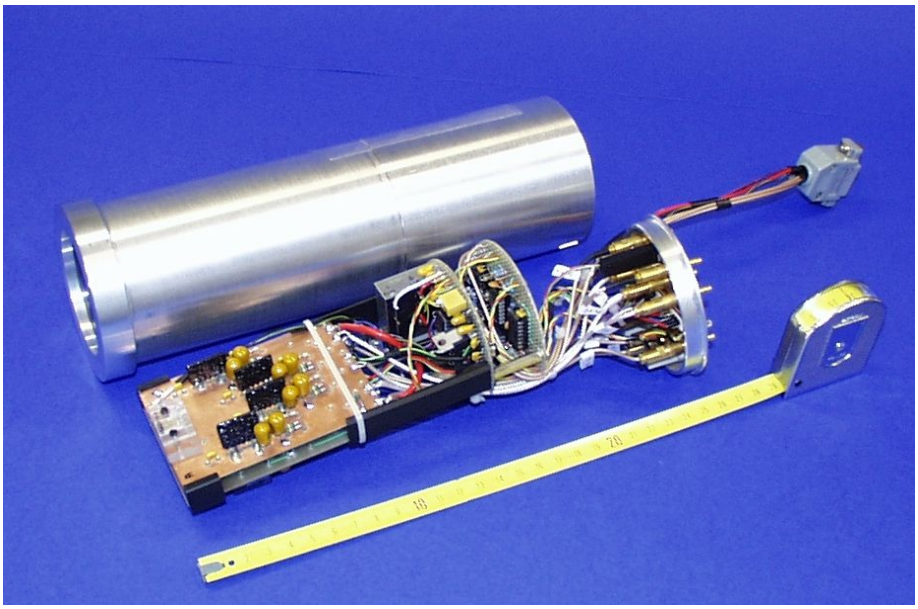

Fig. 6 - CACTμS detecting units housed in a light-tight and airtight container together with the front-end electronics, the voltage supplies, and the housekeeping sensors for remote monitoring. At left, the CdTe sensors containers board including the front-end CSPs; at center, the DC-DC converter and bias filters; at right, the output connectors. (CACTμS collaboration image)

The CACTμS detection unit consists of two CdTe solid-state detector arrays operating at room temperature (see Fig. 13). Each CdTe crystal is divided electrically by a set of four metallic strips deposited on one face, while on the opposite face there is a common electrode connected to ground. The pitch distance between the strip center is 2 mm (1.8 mm wide metallic strip in addition to a 0.2 mm gap). Each strip is a positively biased (nominally +120V) independent electrode on which the charge delivered by an x-ray event is collected and amplified by a conventional Charge Sensitive Preamplifier (CSP). In this way, each CdTe detector is equivalent to four bar-shaped units with a base of 2 mm x 2 mm (orthogonal to the optical axis) and a thickness of 10 mm.

With respect to other former CACTμS' electronics subsystems, our new SSGX payload represents a significant upgrade denoted by a substantial reduction of both the mass and volumetric dimensions of the service electronics. Figure 7 below shows the large dimensions of CACTμS' original 2002 subsystems that included the analog front end electronics (AFEE) box, the Pulse Code Modulation Unit (PCM), the scientific Data Handling System (DHS) with Analogue to Digital Conversion (ADC) and digital control electronics, and the Telecommand/Telemetry unit. These would easily occupy all of the space allotted for the four large payloads as accommodated by HASP. Details are given further below about the current, much smaller integrated electronics systems recently developed at American River College which will interact with the detector unit inherited from the original CACTμS payload.

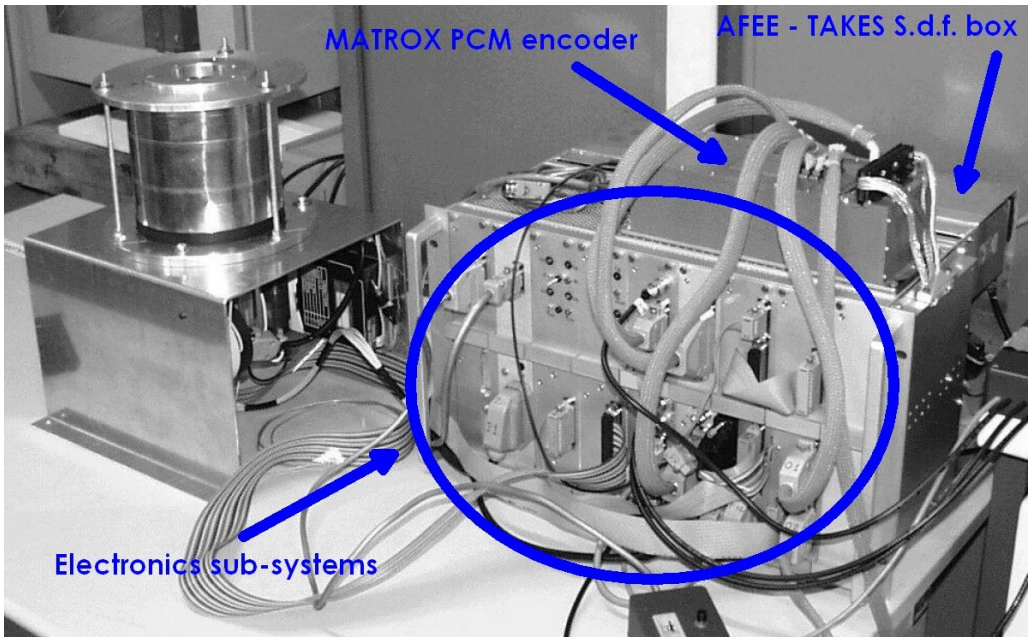

Fig. 7 - Portions of CACTμS electronic subsystems are pictured here. At left, the detecting CdTe units cylinder, which remains with all of the new SSGX payload electronics. The large electronics system indicated by the circle at right has since been replaced by the Data Acquisition/Integrated Storage Interface (DAISI). (CACTμS collaboration image)

With respect to thermal behavior and "housekeeping", all CACTμS systems performed well during the twelve-hour flight; we anticipate similar results from a longer flight. All voltage supplies, including the two voltages biasing the CdTe detector, were continuously monitored during the flight with data transmission in the Telemetry (TLM) format. During the entire flight, none of the monitored voltages deviated from the nominal value by more than twice the quantization uncertainty (±40 mV), thus confirming the reliable operation of all CACTμS subsystems.

The in-flight monitored temperatures deviated from their values at ground due to the thermal gradients with respect to the external environment. Figure 8 below shows the temperature range of the payload electronics and CdTe detector recorded during the flight; the temperature of all other CACTμS subsystems demonstrated a trend similar to those shown in Figure 8.

The detector temperature drift from +28 °C down to approximately -6 °C did not influence the overall detection apparatus, since in-flight automatic gain and offset corrections were continuously performed inside the analog processing electronics. The SSGX DAISI electronics system makes this correction in real time as described in the Payload Electronics section.

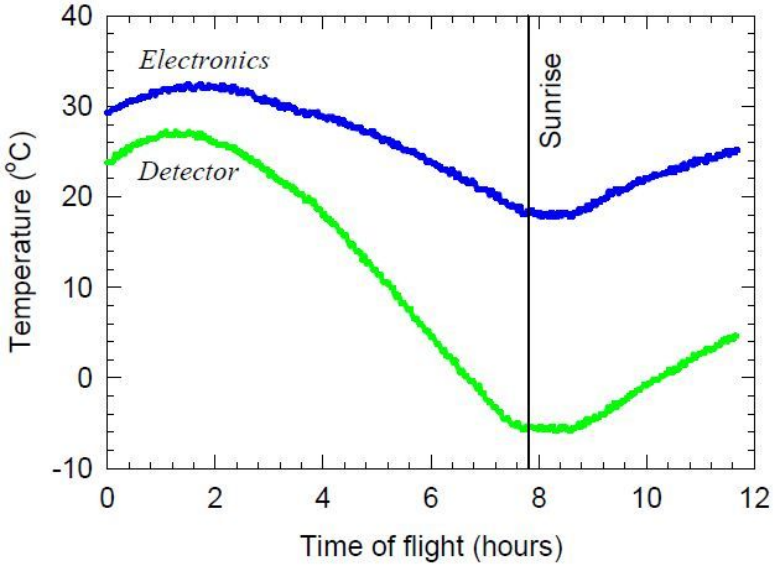

Fig. 8 - The recorded thermal behavior of the CdTe detector and electronics temperature is shown here, expressed as a function of flight time. The balloon was launched at 23:30 local time (Milo, Sicily, Italy), thus flying primarily during cool overnight hours. (CACTμS collaboration graphic)

The entire detector subsystem is contained inside a light-tight aluminum cylinder. Furthermore, all additional subsystems were packed inside a polystyrene box which was then wrapped with Mylar. Although the HASP flight can exceed durations of 20 hours – thus, for substantially longer than the previous twelve-hour flight of CACTμS – a more recent flight of a CdTe sensor over Svalbard, Norway proved equally thermally successful with polystyrene and Mylar thermal protection. Despite the favorable results of the previous flight as well as similar experiments, the new SSGX payload nevertheless applies an active, dedicated thermal protection system as discussed further below.

Finally, we rely on the prior radioisotope ground laboratory energy-channel calibration results of the CACTμS team for in-flight calibration and monitoring of all sensor channel offsets and gains. We will also utilize a "test-in" signal in the CACTμS detector to provide known voltages for real-time calibration. This is necessary to compensate for analog channel gain and offset drift during the flight due to variations in temperature and other environmental parameters such as pressure, humidity, and magnetic field intensity.

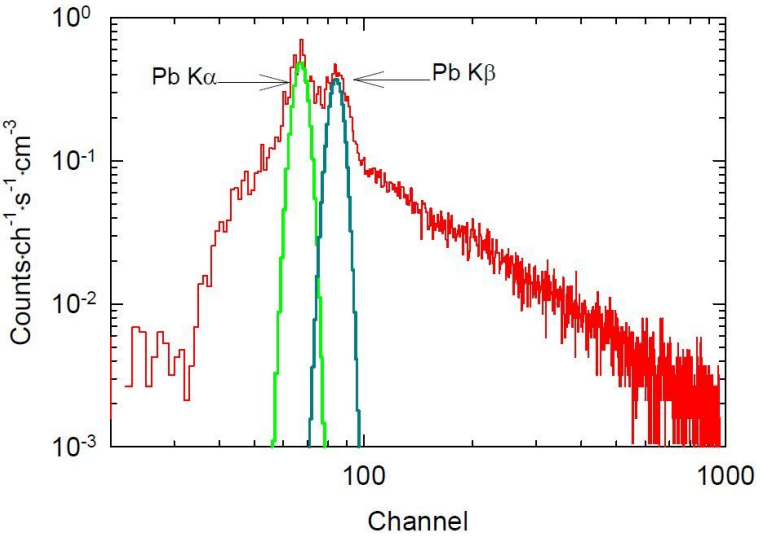

Fig. 9 - This graph shows the energy spectrum detected during CACTµS' flight. (CACTµS collaboration graphic)

1.4 Payload Systems and Flight Operation

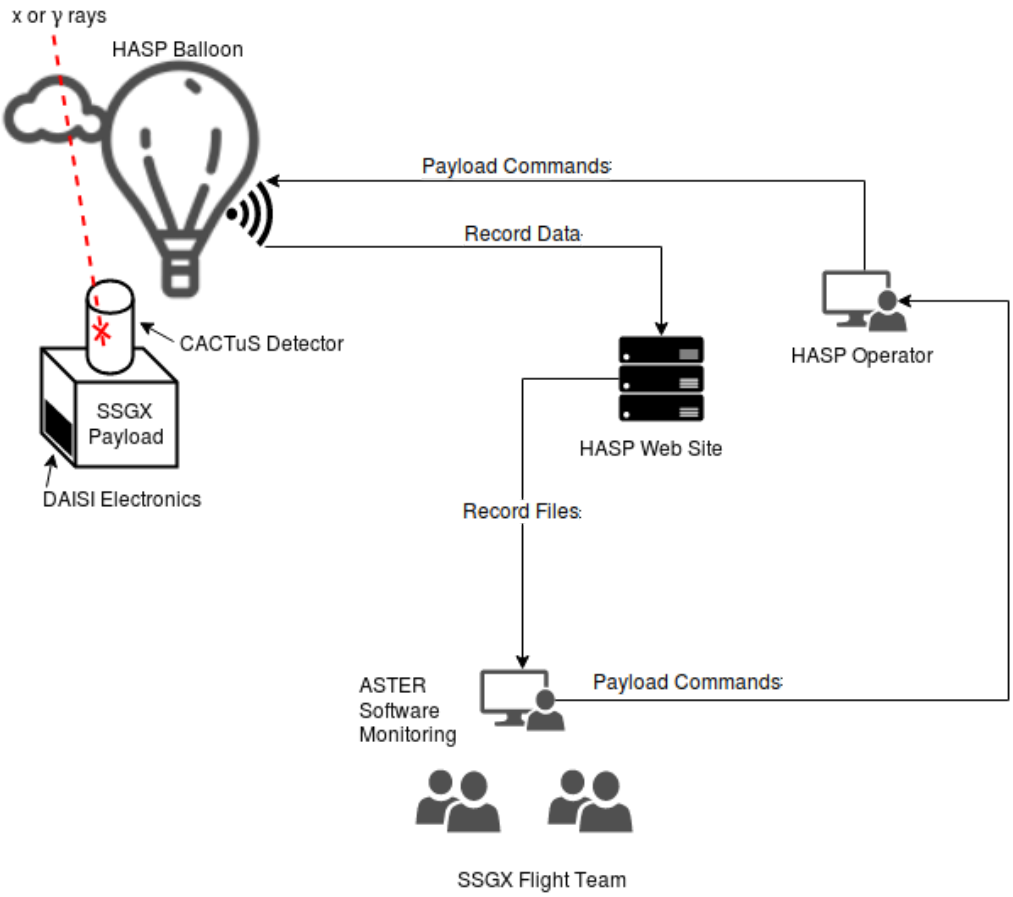

Fig. 10 - The SSGX general system diagram is shown here.

The SSGX payload consists of three major components: the CdTe detector, the DAISI electronics system, and the primary housing structure. In response to x- and γ-ray interactions, the detector outputs analog voltages which are sampled by an analog-to-digital converter within the DAISI electronics system. Data from the detector is then processed and stored via SD card for post-flight analysis. As detailed in the Payload Interface, the primary housing structure secures the detector and electronics to the HASP payload plate. Finally, while not included with the payload itself, the ASTER software utility will perform operations such as system calibration prior to flight, monitoring during the flight (through processing of accumulated data records output by the payload as available on the HASP web site), and some post-flight analysis of data stored on the payload.

1.4.1 Detection System

Fig. 11 - The CACTμS CdTe detection cylinder and cabling are shown here.

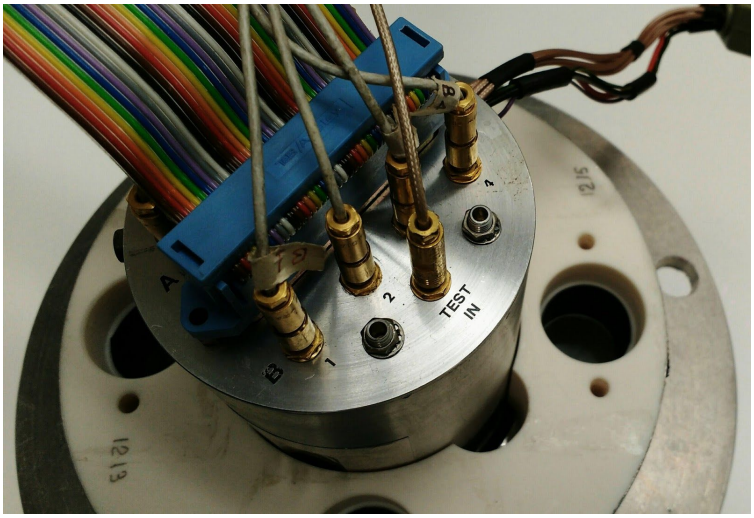

Fig. 12 - A closeup view from the bottom of the detector cylinder, featuring connections.

Cadmium Telluride (CdTe) Detector

The cadmium telluride spectrometers are photovoltaics sensitive to x-ray and γ-ray radiation. When grouped into a pixel array, they can be utilized to determine the intensity, location, and polarization of the measured radiation. The detector consists of two wafers, each split into four strips which independently output an analog voltage dependent on the intensity of the radiation received by the strip. With the wafers stacked and oriented at 90° with respect to each other, the resultant 4x4 pixel grid permits the location of an event to be determined within the detection area. The CdTe detector operates utilizing a 120 V bias, which is generated within the detector cylinder with an EMCO DC-DC converter from a 12 V input.

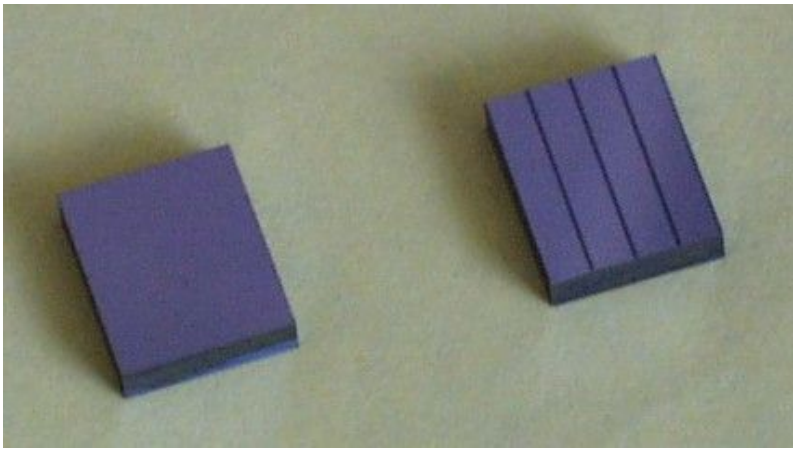

Fig. 13 - ACRORAD (10x10x2 mm^3 sensitive volume) CdTe micro-strip units from the photovoltaic detector. The planar cathode surface is shown at left, the multi-strip segmented anode side at right. The detector has a total of eight channels currently read by an eight channel ADC featuring programmable gain. (CACTμS collaboration image)

1.4.2 Payload Electronics

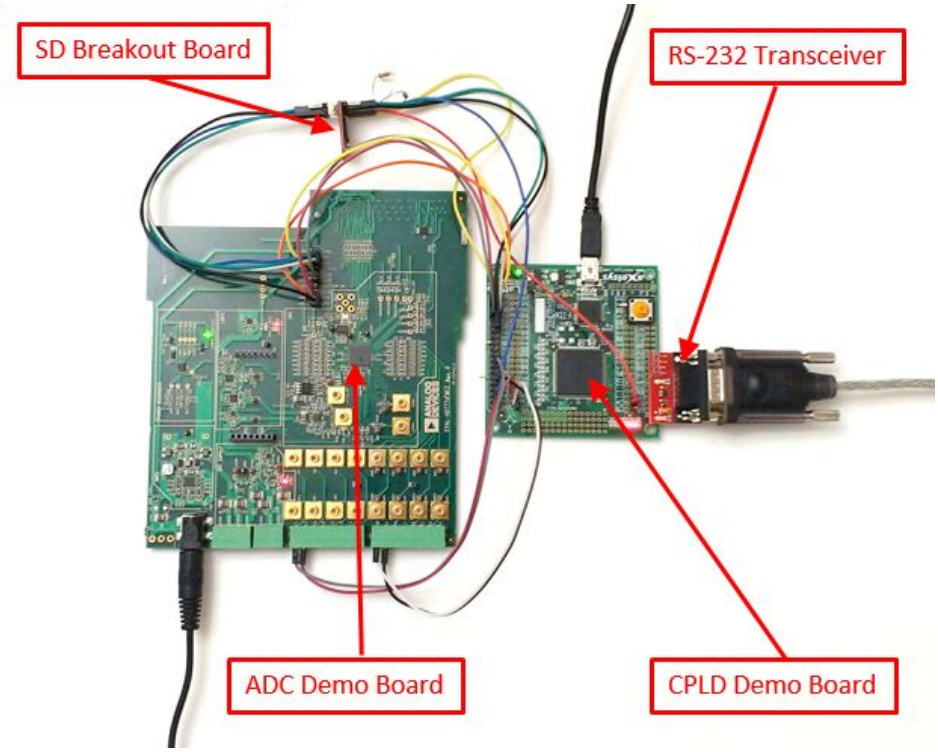

Fig. 14 - The DAISI Prototype is shown here, displaying off-the-shelf demonstration boards from component manufacturers, connected and programmed with early development firmware as a proof of concept for data collection and communication.

DAISI (Data Acquisition/Integrated Storage Interface) is an electronics platform designed by the American River College Physics and Astronomy Club to collect sensor data from multiple sources, monitor and regulate system functionality, and record collected data to SD card. Primary data collected consists of analog voltage levels from the CdTe array, which provides a record of detected x-ray and γ-ray events. Additional data collected includes system voltage levels, detector and electronics temperatures, and system status (e.g. error states). This data is saved in real time to SD card for post-flight evaluation, and instantaneous readings of the system status are transmitted as data records at ten second intervals utilizing an RS-232 interface. The RS-232 interface is further capable of receiving commands to override and adjust automatic functionality. Finally, through monitoring of the electronics temperature, onboard logic can respond by activating resistive heating elements for purposes of thermal regulation, ensuring that all components remain within appropriate thermal tolerances. A brief description of the major electronic components utilized in the DAISI platform is provided below.

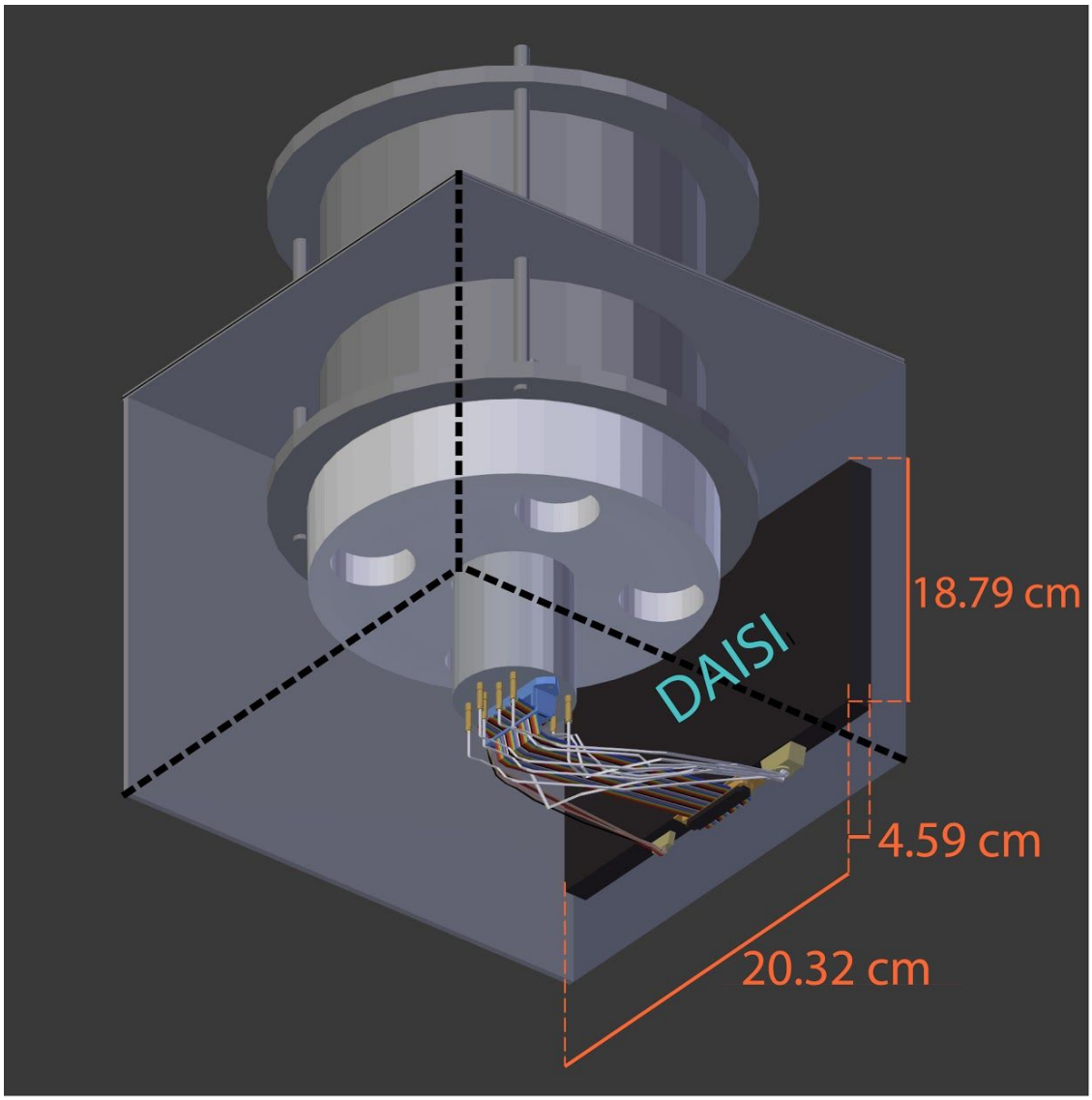

Fig. 15 - The DAISI electronics is housed in an aluminum alloy box, shown here. This enclosure provides shielding against RF interference by radio communication transmissions originating from the HASP platform itself, as well as protection against potential electromagnetic interference induced in the electronics by other payloads.

HASP Interface - Voltage Generation and Communication

The HASP interface connects with the cabling of the HASP balloon, providing the main electrical source of a minimum 29 volts and a maximum 2.5 amps. Additionally, the interface facilitates remote digital communication via RS-232 protocol. Voltage regulators utilize the main voltage supply provided by the HASP interface for generating all local voltage levels required to power all DAISI electronics while simultaneously providing the necessary voltages for the CdTe detector. Many of these regulators may be enabled or disabled by the Complex Programmable Logic Device (CPLD) to manage inrush current at system startup. Regulators may further provide for recovery of error conditions through the power-cycling of individual components during operation. An RS-232 transceiver interfaces with the serial communication port on the HASP balloon for communication with the outside world. It is comprised of a voltage level shifter, which translates the +/- 15 V RS-232 signal voltage from the HASP interface to the 3.3 V range utilized by the CPLD.

Primary Data Collection

The analog-to-digital converter (ADC) is an integrated circuit responsible for the measuring of analog voltage levels from the CdTe detector at a specific point in time, representing that value as a signed 24-bit digital number. Each sample also includes an 8-bit cyclic redundancy check (CRC) value which permits the validation of each sample. The ADC further includes independent programmable gain amplifiers (PGA), allowing for the adjustment of the signal gain for each analog voltage channel. The ADC is capable of sampling at a maximum rate of 16 000 samples/second with included signal-shaping filters based on the selected sampling rate. Additional signal offset and gain can be applied in real time through on-chip diagnostic functions and the detector test interface, allowing for signal corrections over time in response to changes due to variations in environmental conditions.

Data Processing

A CPLD is a general-purpose digital circuit made up of numerous configurable blocks that can be programmed to perform multiple custom operations simultaneously. For the purposes of this project, the CPLD manages system startup, collects the regular readings of digital ADC output values, collects detector and electronics temperatures, samples all regulator voltage levels, and packages these readings into a standard format that is written to the onboard SD card storage device. The CPLD also utilizes temperature data from the electronics to determine when heating elements should be activated in order to ensure that all components remain within the temperature tolerance necessary for operation. The CPLD monitors the RS-232 interface for incoming data commands and regularly transmits data records through the HASP communication interface.

Data Storage
DAISI includes an SD card interface which acts as the permanent data storage device for all collected data written by the CPLD. This data includes the CdTe sensor analog voltages, detector and electronics temperature data, regulator voltage levels, and system status. Data is written to the SD card in 512-byte data blocks at a rate of 0.386 MB/s. Industrial temperature grade SD cards hardened for x-ray exposure are employed for this system, with two SD cards utilized simultaneously for the purpose of data redundancy. Data stored via SD card is retrieved after the flight and examined with PC-side software for scientific analysis.

1.4.3 Firmware Design

CPLD: Overview
The CPLD is the main processing unit within the DAISI electronics platform. It simultaneously acquires and saves data, determines system performance, and responds to changes in device status. Broadly, a CPLD is a general-purpose digital circuit made up of numerous configurable blocks that can be programmed to perform many custom operations concurrently. CPLDs provide multiple benefits absent from microprocessor options, including low power operation, high clock rates, and truly simultaneous processing capabilities. Logic for the CPLD is coded using the Verilog programming language, which has been divided into functional modules as pictured below.

As mentioned in Data Processing, the CPLD manages system startup, collects the regular readings of digital ADC output values, collects detector and electronics temperatures, samples all regulator voltage levels, and packages these readings into a standard format that is written to the onboard SD card storage device. The CPLD further relays components for thermal regulation, monitors the RS-232 interface for incoming data, and responds to commands from the HASP communication interface.

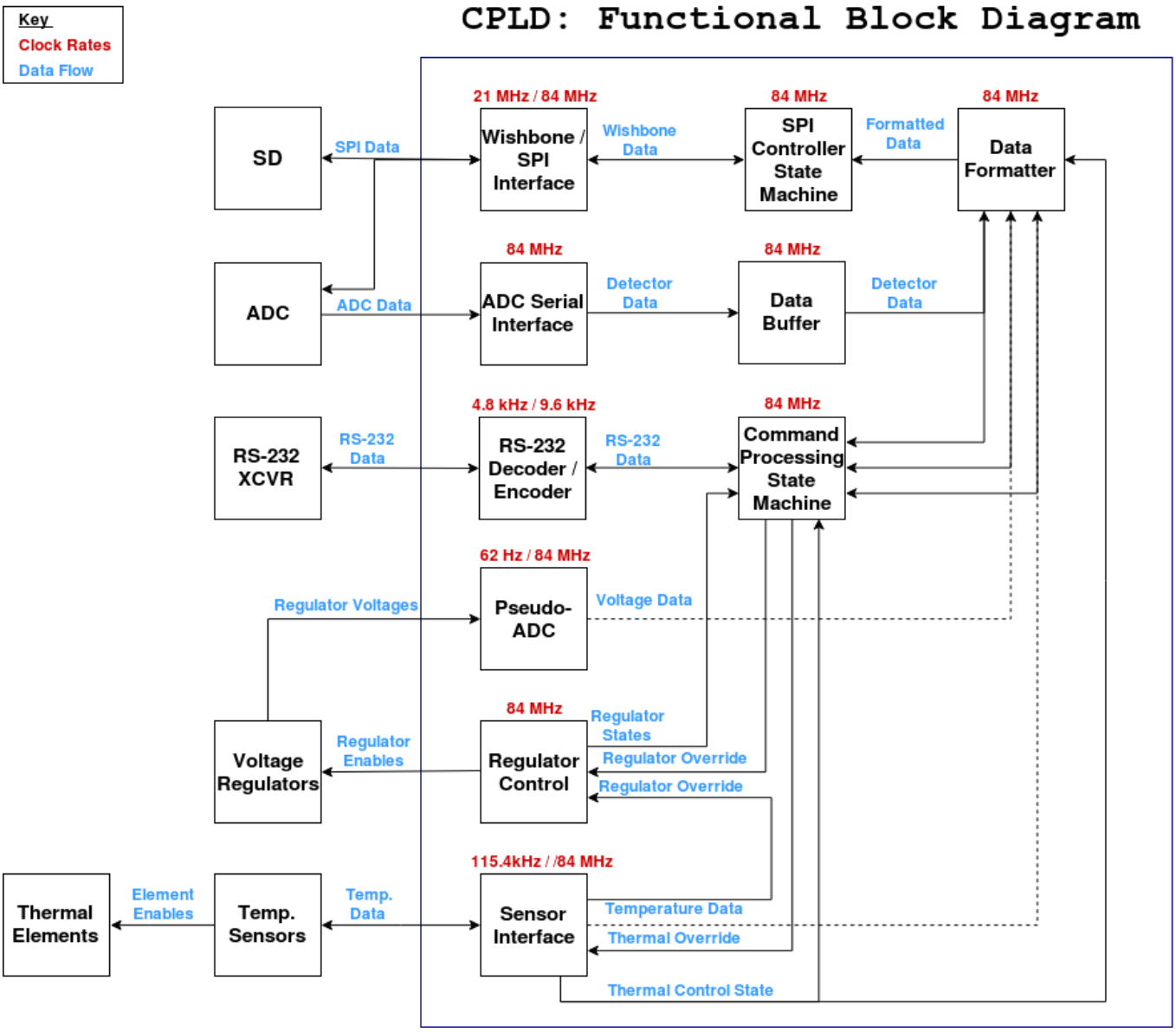

Fig. 16 - This block diagram details the internal CPLD modules which have been coded to simultaneously process incoming information and distribute data among the modules.

1.4.4 Thermal Control

Temperature Sensors
Thermal sensors measure local temperatures for both the DAISI electronics and the CdTe detector cylinder. Four temperature sensors are integrated into the DAISI electronics. Each operates over a range of -55 ºC to +125 ºC with 14-bit resolution and includes programmable output pins. These outputs will be utilized for active temperature regulation by toggling switches connected to resistors used for heat dissipation.

Heating Elements
Thermal regulation of DAISI electronics is achieved by a set of resistive heating elements which can be actively enabled or disabled by the CPLD through the temperature sensor local to the element. The final custom Printed Circuit Board (PCB) will contain four of these regulation circuits, with one placed at each corner of the PCB. Resistive heating elements will conduct thermal energy through planes of copper within the PCB, directly heating the electronic components. When active, each resistive element will contribute up to +36 ºC differential to ambient temperature through power dissipation of 8 W. Along with the heat dissipation from voltage regulators, the active heating elements will function like a thermostat by enabling heating elements when the temperature drops below -20 ºC. This maintains operative temperature in the electronics well above the minimum absolute temperature threshold of the constituent devices.

1.4.5 Anticipated Software Development

Aggregate Software for Technical Execution and Retrieval (ASTER): Overview
ASTER is a user interface programmed in Java by the American River College Physics and Astronomy Club for the purpose of interacting with DAISI in order to translate collected data into its graphical representation. The software will process payload record files as they become available during the flight. ASTER will also operate as a front-end software for reviewing the SSGX operation as various status updates are parsed from record files, presenting the accumulated data transmitted from the payload during the flight and display operation status over time.

ASTER will be used during development to calculate calibration corrections to compensate for any anomalous data. The program uses data extracted from the SD card to generate plots in order to graph energy spectra, single/double events, and to visualize the pixel map. All extracted data may also be saved for later viewing in a Comma-Separated Values (CSV) file. Furthermore, ASTER will provide a zoomed-in, windowed display capable of scrolling the graph along a timeline in order to observe specific sections of data. ASTER is capable of extracting and utilizing data from all eight analog channels. When prompted, the program will convert accumulated data values to voltages and display a scatter plot of the incidental voltages.

II. Team Structure & Management

In June 2014 the ARC Physics and Astronomy Club successfully launched and retrieved a 3 kg payload balloon in California's Mojave Desert. With a flight duration of approximately two hours, the balloon was equipped with commercial GPS, flight cameras, and an aerogel chamber for microbial capture. Components were controlled via Raspberry Pi microcomputer, utilizing Python code developed by the group. Focused on developing a praxis of balloon flight at American River College, the club learned about HASP in 2014 and subsequently established a collaboration with our experienced senior partners in Italy and Portugal. The Portuguese and Italian team members have an existing collaboration dating for more than a decade, having developed a number of joint projects in astronomy.

The current student-based team at American River College consists primarily of S.T.E.M. undergraduates who have significantly expanded the work from previous years. In order to advance the interests of this project, the group has been meeting for several hours each week since March 2017. Working individually and in groups, students have been developing skills in firmware and logic design, software design and development, schematic design, technical illustration and CADD, simulation development, and hardware assembly.

The student team is coordinated by the project and electronics leaders. Team communication occurs almost daily via SMS group messages and e-mail correspondence. Furthermore, the student group meets at the ARC campus library and at private residences for several hours each week to brainstorm, share updates, and seek feedback. The project faculty coordinator meets at ARC once weekly with students for a progress review, general management, and troubleshooting.

Coordination of the international team is managed through a combination of e-mail correspondence between the ARC student electronics lead and CACTμS contributors as well as e-mail correspondence and Skype teleconferences held among all faculty senior members in Portugal, Italy, and the USA. Furthermore, all members of the SSGX project team have access to live document editing via shared cloud storage, including documentation for the proposal and for ongoing development. A project task list is currently undergoing conversion to a spreadsheet document with clearly marked deadlines and progress monitoring.

More specifically, ARC got started in GEANT with help from the Portuguese team members who provided several files and template code for developing a specific SSGX detector's geometry simulation. Since that time, additional Portuguese students have joined the team with goals of both learning and contributing to software development for the post-flight data processing.

Contributions from Italian team members include the CACTμS equipment from 2002 and related reporting on all its functionality details. More recently, before shipping the detector and part of its electronics to the USA, the Italian members took lab-based spectroscopic measurements to quantify the differences in efficiency between the CdTe detector anode groups. The figure below illustrates one such measurement.

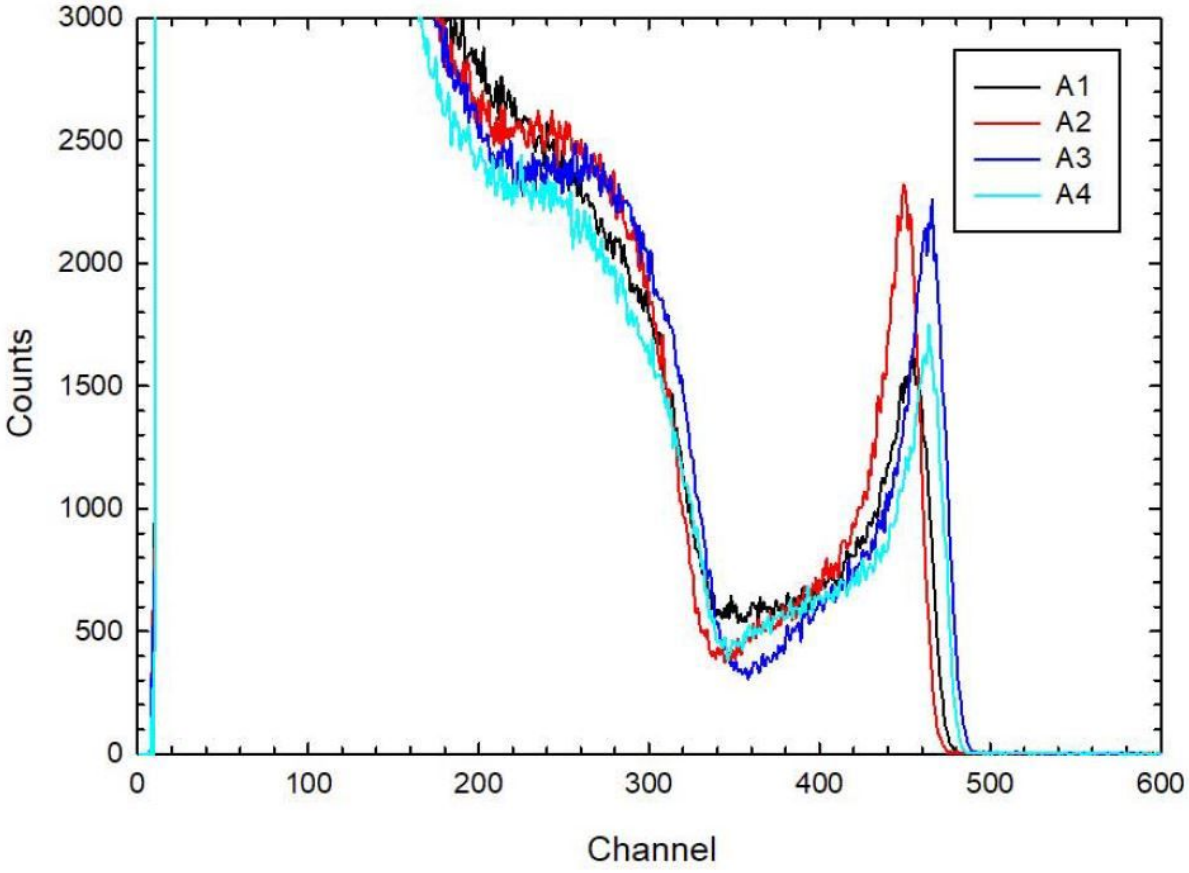

Fig. 17 - Spectroscopic measurements provided by Italian team members are displayed here. For the CdTe sensor A, anode strip 1 to 4, this is the spectra of ^{137}Cs integrated over one hour live time. Differences in efficiency (of about 10%) between anode groups (1,4) and (2,3) are mainly due to the fact that 1 and 4 are the external anodes (border effect) of the sensor.

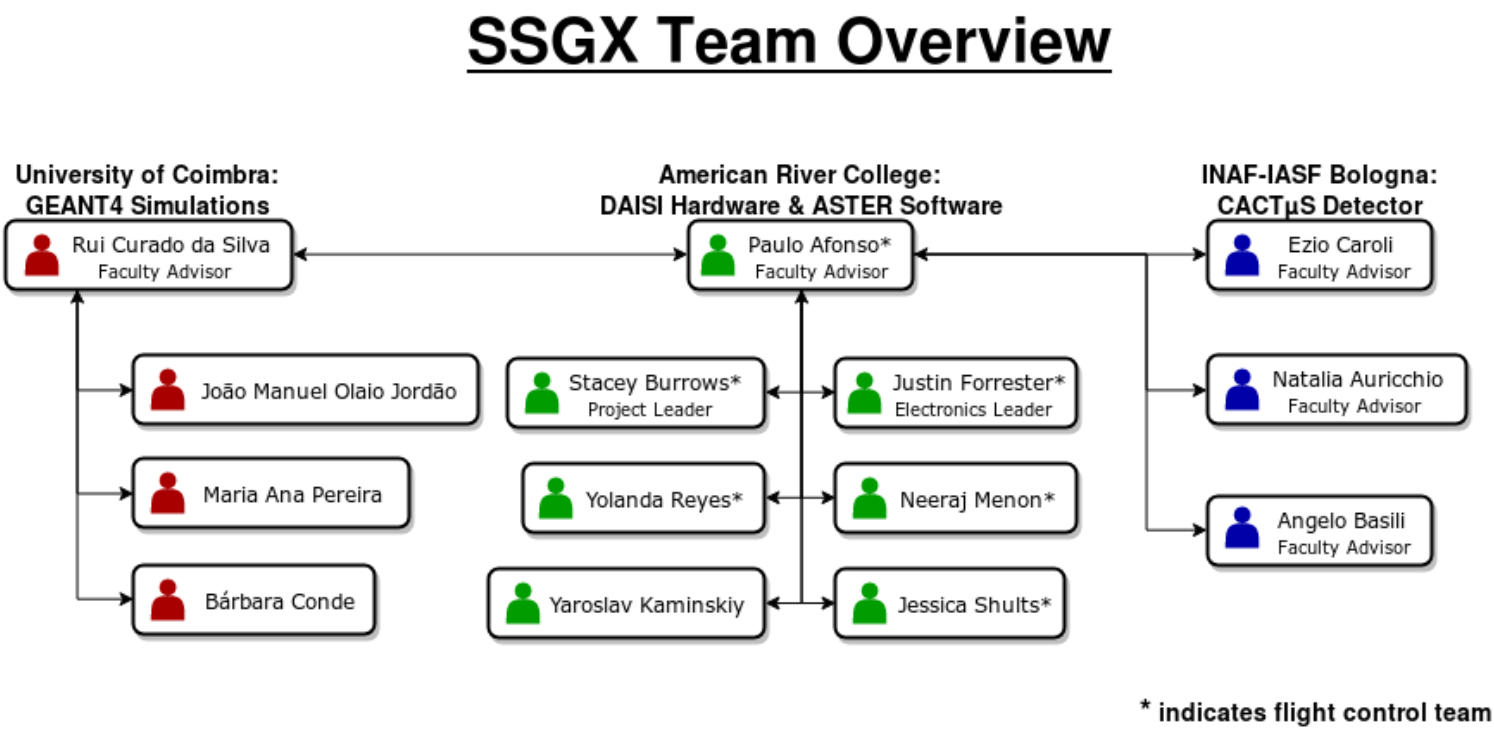

Fig. 18 - This tree shows the structure of the international SSGX project team.

Table 1: Project Contributors

Name (Institution)	**Title**	**Additional Roles**	**Contact Information**
Paulo Afonso * (ARC)	Faculty Advisor	Project coordination, researcher	afonsop@arc.losrios.edu (916) 484-8733
Rui Curado da Silva (University of Coimbra, Physics Dpt. - LIP)	Faculty Advisor	GEANT4 simulations and data analysis, researcher	rui.silva@coimbra.lip.pt +351 239 410663
Ezio Caroli (INAF-IASF Bologna)	Faculty Advisor	CACTµS collaboration, researcher	caroli@iasfbo.inaf.it +39 051 6398678
Natalia Auricchio (INAF-IASF Bologna)	Faculty Advisor	CACTµS collaboration, researcher	auricchio@iasfbo.inaf.it +39 051 6398779

Angelo Basili (INAF-IASF Bologna)	Faculty Advisor	CACTμS collaboration, technical personnel	basili@iasfbo.inaf.it +39 051 6398674
Stacey Burrows ***** undergraduate (ARC)	Project Leader	Schematic design, block diagrams	stacey.a.burrows@gmail.com (916) 712-1878
Justin Forrester ***** B.S. in CPE (CSU Sacramento) undergraduate: science (ARC)	Electronics Leader	Logic design, block diagrams, researcher	justin.forrester@gmail.com (916) 462-7047
Neeraj Menon ***** undergraduate (ARC)	Software Developer	Logic design collaboration	neerajmenon95@gmail.com
Yolanda Reyes ***** undergraduate (ARC)	Technical Illustrator	Simulation development, materials	w1606799@apps.losrios.edu
Jessica Shults ***** undergraduate (ARC)	Assembly Technician	Astronomy Club Secretary	jessica.marie.shults@gmail.com
Yaroslav Kaminskiy undergraduate (UC Berkeley, transfer from ARC)	Simulation Developer	Astronomy Club contributor	yaroslavk@berkeley.edu
João Manuel Olaio Jordão MSc. student (University of Coimbra)	Software & data analysis	Post-flight data treatment	joaojordao.97@gmail.com
Maria Ana Pereira MSc. student (University of Coimbra)	Software & data analysis	Post-flight data treatment	mariafonsopereira@gmail.com
Bárbara Conde undergraduate (University of Coimbra)	Software & data analysis	Post-flight data treatment	mysnij@gmail.com

*** indicates flight control team**

Table 2: Anticipated HASP 2018 Development Timeline

Date	**Development Goal**
December 2017	● Complete and submit HASP application ● Evaluate and refine detector signal shaping ● Evaluate prototype performance over long sampling times ● Validate and finalize all circuit schematics ● Complete initial PC software control interface
January 2018	● Complete PCB layout and submit for manufacturing ● Complete PC software windowed scatter plots for all sensor types ● Submit monthly status report
February 2018	● Assemble and validate all PCB subsections ● Complete electronics noise minimization ● Complete PC software visualization for all desired plot types ● Acquire all required materials for main housing assembly ● Submit updated proposal based on reviewer feedback ● Submit monthly status report ● Attend HASP teleconference
March 2018	● Complete initial pressure and temperature testing ● Complete all detector sensor readout calibrations using high-energy photon emissions ● Complete PC software calibration interface ● Complete mounting bracket installation onto mounting plate ● Submit monthly status report ● Attend HASP teleconference
April 2018	● Complete and validate automatic in-flight calibration adjustment routines based on software calibration results ● Assemble main SSGX housing ● Submit preliminary PSIP document ● Submit monthly status report ● Attend HASP teleconference
May 2018	● Finalize documentation of SSGX dimensions and detailed integration plan for submission ● Finalize documentation of DAISI electrical properties ● Submit monthly status report ● Attend HASP teleconference
June 2018	● Prepare for payload integration ● Submit final PSIP document ● Submit monthly status report ● Attend HASP teleconference

July 2018	● Complete payload integration at CSBF ● Submit final FLOP document ● Submit monthly status report ● Attend HASP teleconference
August 2018	● HASP flight preparation ● Target flight ready ● Target launch date and flight operations ● Payload recovery and shipping ● Begin post-flight data analysis ● Submit monthly status report ● Attend HASP teleconference
September 2018	● Submit final monthly status report ● Attend HASP teleconference ● Continue post-flight data analysis
October - November 2018	● Perform post-flight data analysis ● Complete data analysis required for HASP science report ● Complete flight and science report
December 2018	● Submit final flight / science report

III. Payload Interface

3.1 Payload Dimensions

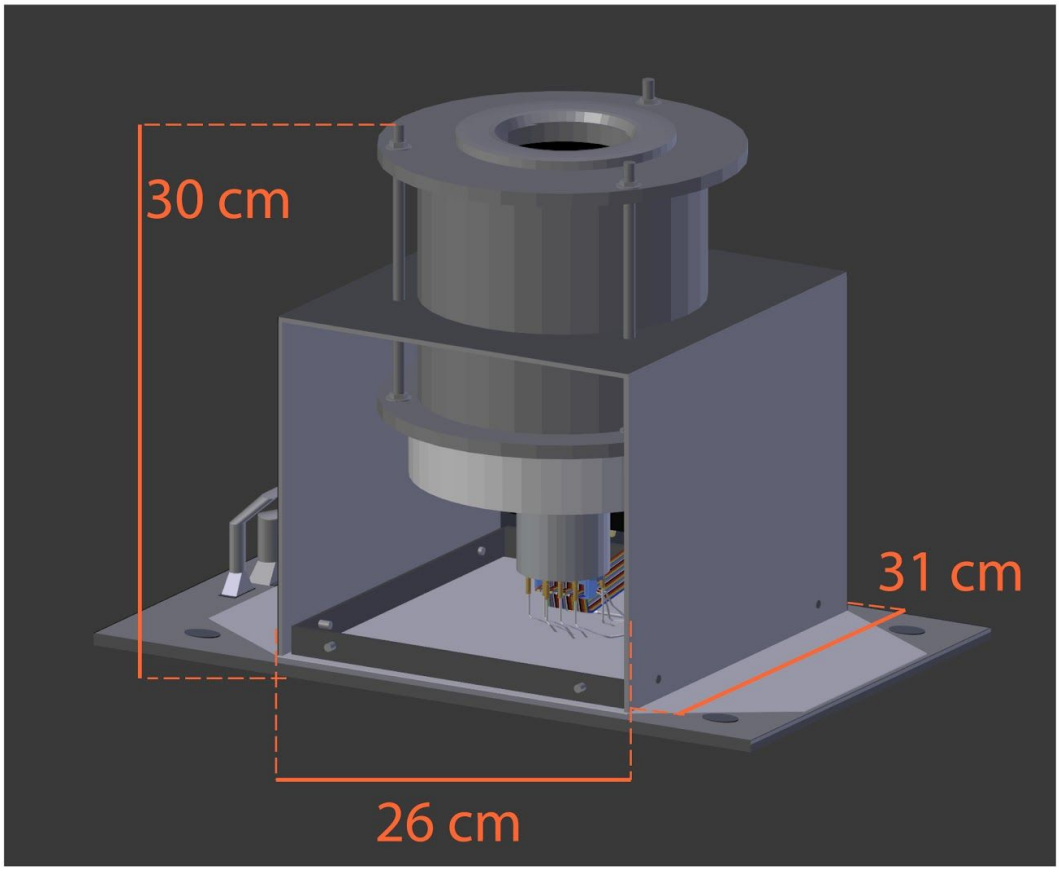

Fig. 19 - SSGX payload dimensions are shown here.

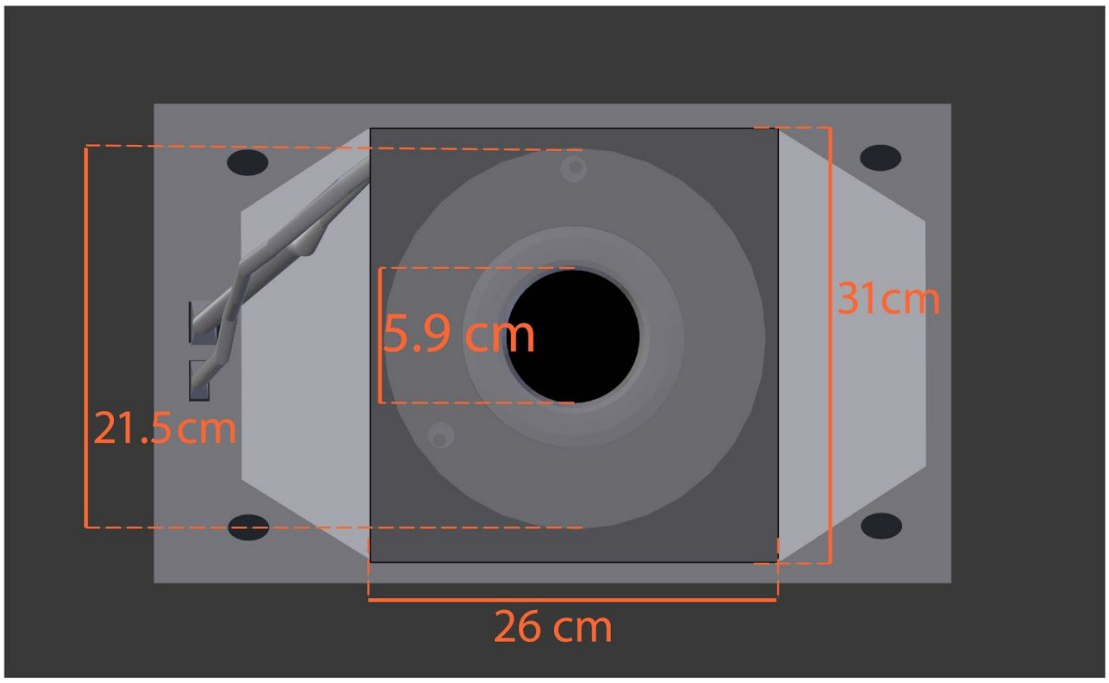

Top view of SSGX payload mounted on HASP

Illustration by Yolanda Reyes

Fig. 20 - Top view of the SSGX payload mounted on the HASP platform.

3.2 Weight Distribution

Table 3: Weight Budget

Component	**Mass (kg)**	**Uncertainty**	**Value Source**
Detector Cylinder with Cables	5.90	+/- 0.1 g	Measured with digital scale
Payload Housing	3.50		Calculated based on material datasheet and quantity of material required
DAISI Electronics (prototype)	0.15	+/- 0.1 g	Measured with digital scale
Electronics Shield	0.44	+/- 0.1 g	Measured sample of approximate expected dimensions

Total (kg)	**9.99 kg**	**+/- 0.2 g**

3.3 HASP Integration Plan

Using Weld-on 2007 solvent cement for rigid and foamed vinyl, we will cement and mount a 4.57 cm tall PVC bracket to the provided 0.635 cm thick HASP payload plate. We will use eight 1.9 cm 8-32 flathead screws to attach the main payload housing, including the CdTe detector, to the cemented PVC bracket. These screws will be placed 2.54 cm away from adjacent seams, and 1.27 cm above the HASP payload plate. SSGX may be mounted on any of the large payload positions, therefore we are not requesting a specific location on the platform.

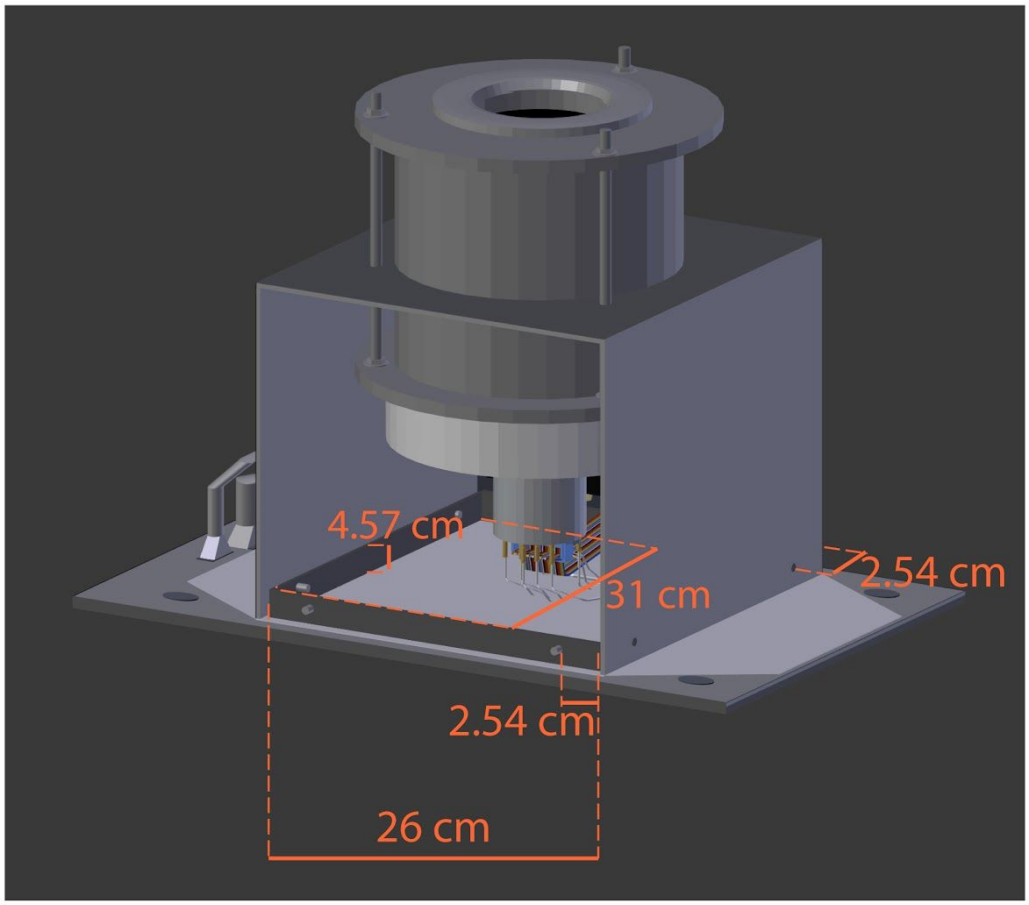

Side view of SSGX payload mounted on HASP

Illustration by Yolanda Reyes

Fig. 21 - Side view of the SSGX payload, featuring mounting dimensions.

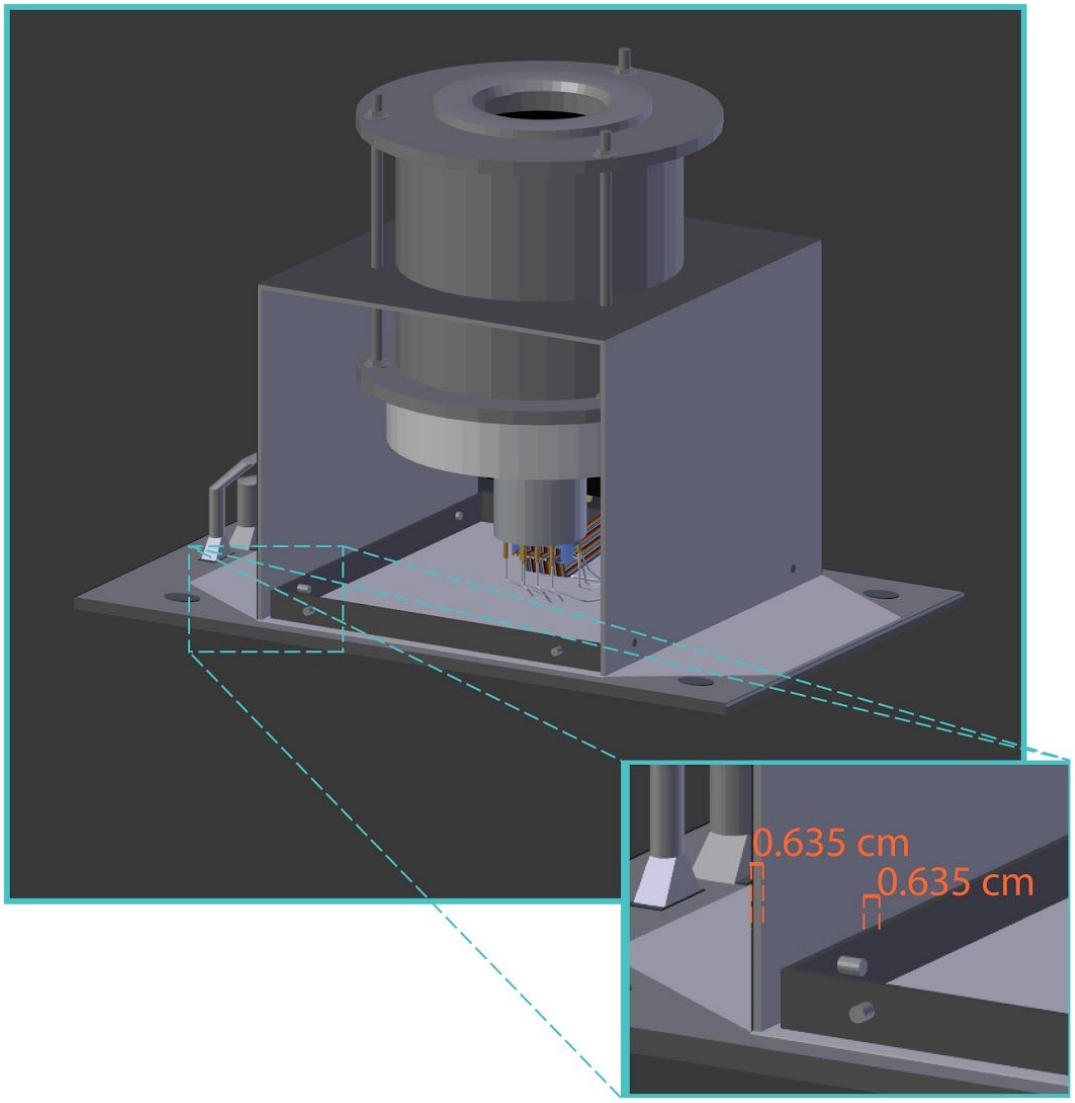

Fig. 22 - Side view of the SSGX payload, detailing the mounting bracket.

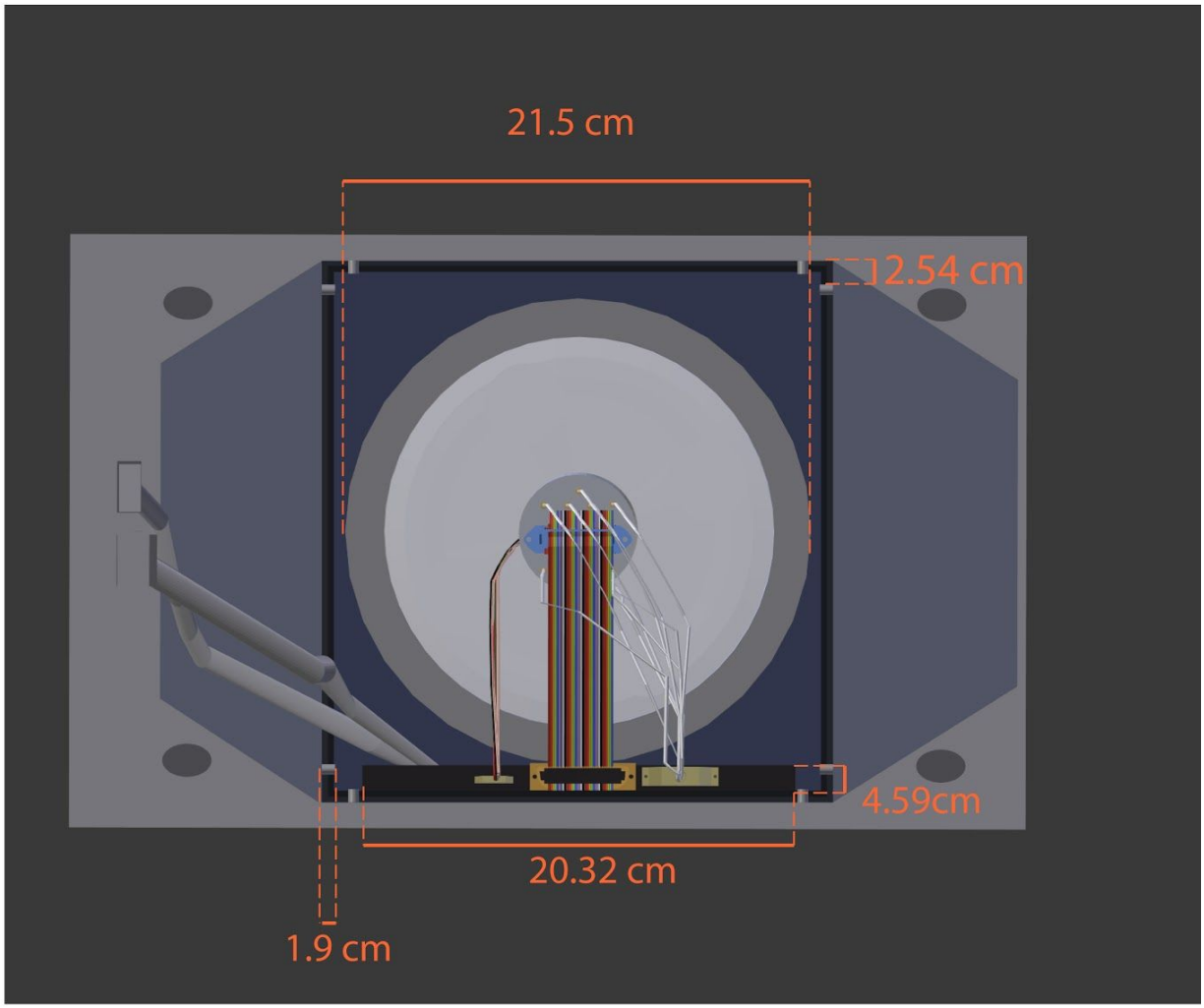

Bottom view of SSGX payload mounted on HASP

Illustration by Yolanda Reyes

Fig. 23 - Bottom view of the SSGX payload mounted on the HASP platform, with the HASP mounting plate made transparent to indicate specific placement.

SSGX Electrical Connections to HASP
EDAC and DB9 connectors from the HASP mounting plate provide pigtail wires for electrical access. The DAISI electronics includes a 5-pin wire terminal header to connect to the pigtail wires from the mounting plate. The table below indicates which connections are utilized by this project.

Table 4: Platform Connections Pin-Out

Header Pin	Label	HASP Pin
1	30 V Power	A, B, C, D (EDAC)
2	Power Ground	W, T, U, X (EDAC)
3	RS-232 Receive	2 (DB-9)
4	RS-232 Transmit	3 (DB-9)
5	RS-232 Ground	5 (DB-9)

3.4 Electrical Distribution

Voltage Regulators
These components utilize a main voltage supply of 29-33 V from the HASP interface to generate all local voltage levels required to power the DAISI electronics, in addition to providing the necessary voltages for the CdTe detector. Many of these regulators may be enabled or disabled by the regulator control module to manage inrush current at system startup through the staggered powerup of individual circuits, and/or to provide for recovery of error conditions through the power-cycling of individual components during operation. A CPLD module determines when the external voltage regulators are turned on or off. At startup, it will stagger the initiation of each regulator to limit the inrush current when DAISI is first powered. After startup, individual regulators may be enabled or disabled in response to events, such as for the need to power-cycle a device in the event of a communication failure, or in response to commands received by the command processor.

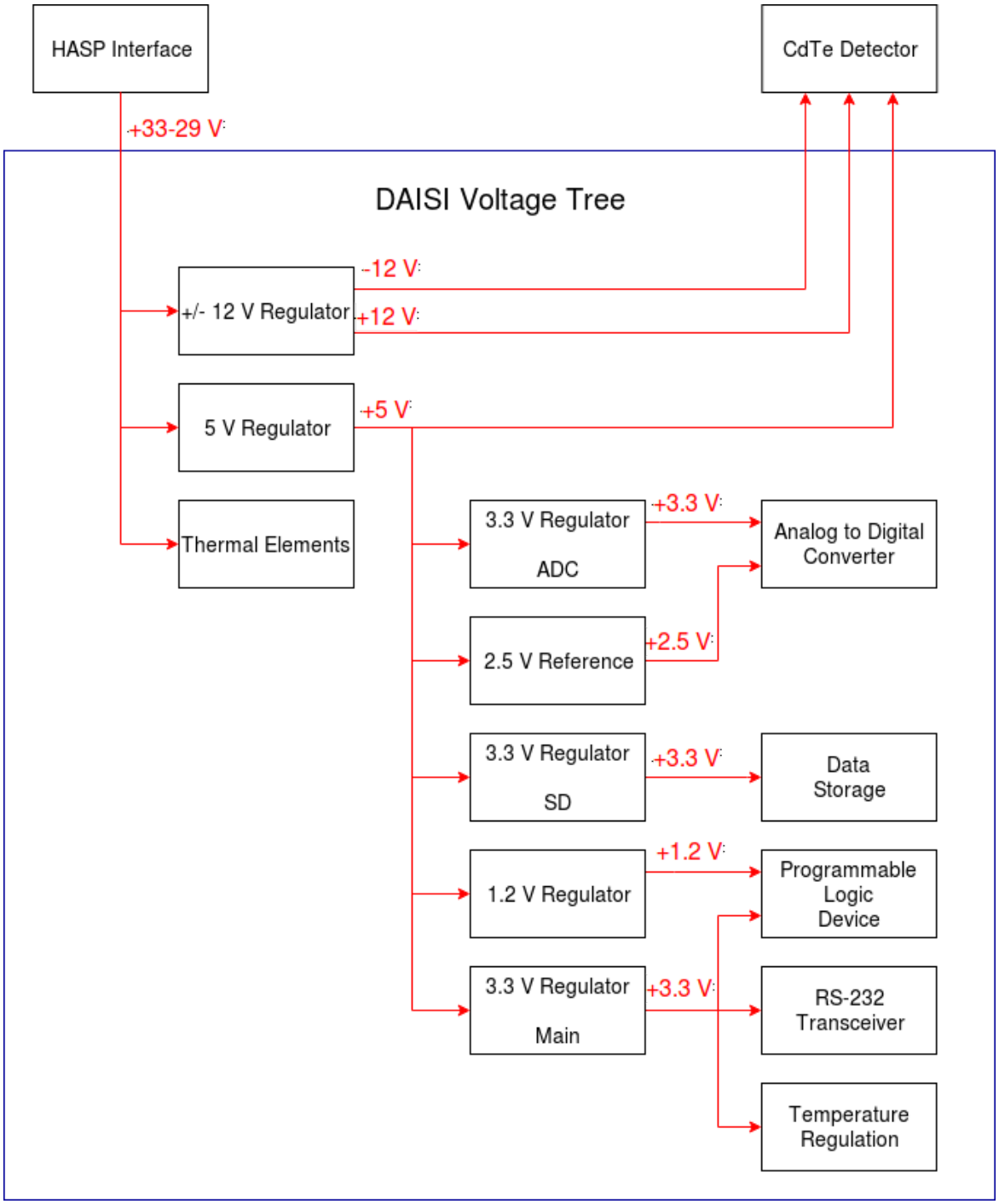

Fig. 24 - Voltage distribution tree indicating which voltage regulators are used to supply power to individual components.

Voltage Monitoring

The voltage output from each onboard regulator is passed through a resistor-divider circuit and used to charge a capacitor connected to a CPLD input/output (IO) line. The capacitor charge time is used by a pseudo-ADC module coded within the CPLD to determine the regulator output voltage levels while the device is operating. This element functions as a low-precision ADC implemented in Verilog and is used to verify the voltage levels output by the various voltage

regulators throughout DAISI without needing to provide additional measurement components. The CPLD obtains a digital voltage reading by driving an IO line low in order to discharge the external capacitor, then switches the IO line to a high-impedance state and increments a counter until the voltage on the IO line reaches the threshold necessary for the line to be read as "high." A greater voltage will require less time to reach this threshold value, allowing the voltage level to be determined. This process is continuously repeated and the results are averaged to produce a final reading at the desired rate.

Component Current Requirements

The HASP platform provides a maximum 2.5 amps to power payload electronics. Table 5 below breaks down the expected current draw from the major components of the system and demonstrates how the SSGX system will remain below the maximum current permitted. Since the printed circuit board for the DAISI electronics is finalizing development, many component current draw values are obtained from datasheets. Where applicable, the total current draw from the vender demonstration boards has been measured while performing DAISI operations and is included below.

Table 5: Current Consumption

Component	Max Used (mA)	Uncertainty	Source
Detector	200	+/- 10 mA	Provided by CACTμS team.
CPLD	14.35		Calculated using vender tool for the current logic implementation. The CPLD demo board uses 79 mA +/-1 mA total.
ADC	47.65		Calculated using maximum specified in datasheet. The ADC demo board uses 121 mA +/-1 mA total.
SD x 2	200		Calculated using maximum specified in datasheet when device is active.
RS-232 Transceiver	1	+/- 1 mA	Measured using bench supply.
Temp Sensor x 4	1.6		Calculated from datasheet.
Thermal Element x 4	1033	+/- 10 mA	Calculated based on resistor datasheet for desired thermal dissipation.

Total (mA)	**1496.6 mA**	**+/- 15 mA**

3.5 Communication Plan

RS-232 Command Processing

Data is received and transmitted through the transceiver, assuming a start and stop bit without flow control, at a rate of 4800 baud. Within the CPLD, an encoder/decoder module receives the serial data from the RS-232 transceiver in the RS-232 protocol format and makes it accessible as a series of bytes to a command processing module. Oversampling the incoming data at a rate of 4x in order to detect bit transitions accounts for possible clock speed differences between DAISI and the HASP platform. The command processor accumulates incoming bytes and detects combinations which pass checksum verification and are determined to represent commands routed to the correct payload. As demonstrated in the table below, DAISI utilizes the payload command format suggested by HASP. Detection of a valid command will trigger a state change in the system, such as restarting a component to recover from an error state. Additionally, the command processor generates status update records at ten second intervals, passing this string to the encoder/decoder module for transmission.

Table 6: HASP Command String and Student Payload Command Format

Byte	Hex Value	Description
1	1	Start of Heading (SOH)
2	2	Start of Text (STX)
3	Command byte 1	Bits 0-3: Command Checksum Bits 4-7: Payload Number
4	Command byte 2	Command Value
5	3	End of Text (ETX)
6	D	Carriage Return (CR)
7	A	Line Feed (LF)

Status Update Records

These 88 byte records provide a snapshot of the overall system status including information such as the current detector ADC readings and current regulator voltages. As such, instantaneous data from most modules is provided to the command processor so that this data is available for system updates. Additional information includes events accumulated since the previous update, such as single and double event counts and number of detected errors. The record also indicates what the last two byte serial command was and the current execution status of the command if it was detected to be valid.

Table 7: Status Update Record Format

Bytes	Description
1-4	Record Sequence Number
5-8	Checksum
9-40	4 byte detector ADC values for all eight channels (32 bytes total)
41-56	2 byte regulator voltage values for four regulators (16 bytes total)
57-64	2 byte temperature values for four sources (8 bytes total)
65-70	6 byte single event count since last update
71-76	6 byte double event count since last update
77-84	2 byte device error codes for four sources (8 bytes total)
85-88	4 byte last command received value and command execution status

Maximum Communication Rate

Including both the record header and payload data, the maximum number of bytes transferred per update is 88. This allows for an update on the instantaneous detector analog voltages, single and double event counts, system regulator voltages, temperature sensor readings, and the occurrence of any error states without approaching the maximum data throughput allotted by the 4800 baud connection. In response to adverse system conditions, the team may occasionally send 2-byte payload commands as the HASP operator is available.

Table 8: Current DAISI RS-232 Command List

Voltage Regulator Reset/Disable Controls	
Command Byte Format	**Description**
Bits 5-8: 0 in hexadecimal Bit 4 Bits 3-1: Voltage Regulator ID	The voltage regulator associated with the designated ID is either restarted if state equals 1 or disabled if state equals 0

Thermal Regulation Reset/Disable Controls	
Command Byte Format	**Description**
Bits 5-8: 1 in hexadecimal Bit 4: State Bits 3-1: Thermal Regulator ID	The thermal regulator associated with the designated ID is either restarted if state equals 1 or disabled if state equals 0

Start/Stop ADC Sampling	
Command Byte Format	**Description**
Bits 5-8: 2 in hexadecimal Bit 4-1: State	The reset command sequence for the ADC is triggered if state equals 1 or the ADC is disabled if state equals 0

Reset System	
Command Byte Format	**Description**
Bits 8-1: FA in hexadecimal	System immediately initiates the rebooting sequence, placing all components back to the default operational state

IV. Preliminary Drawings

4.1 Payload and Platform Integration

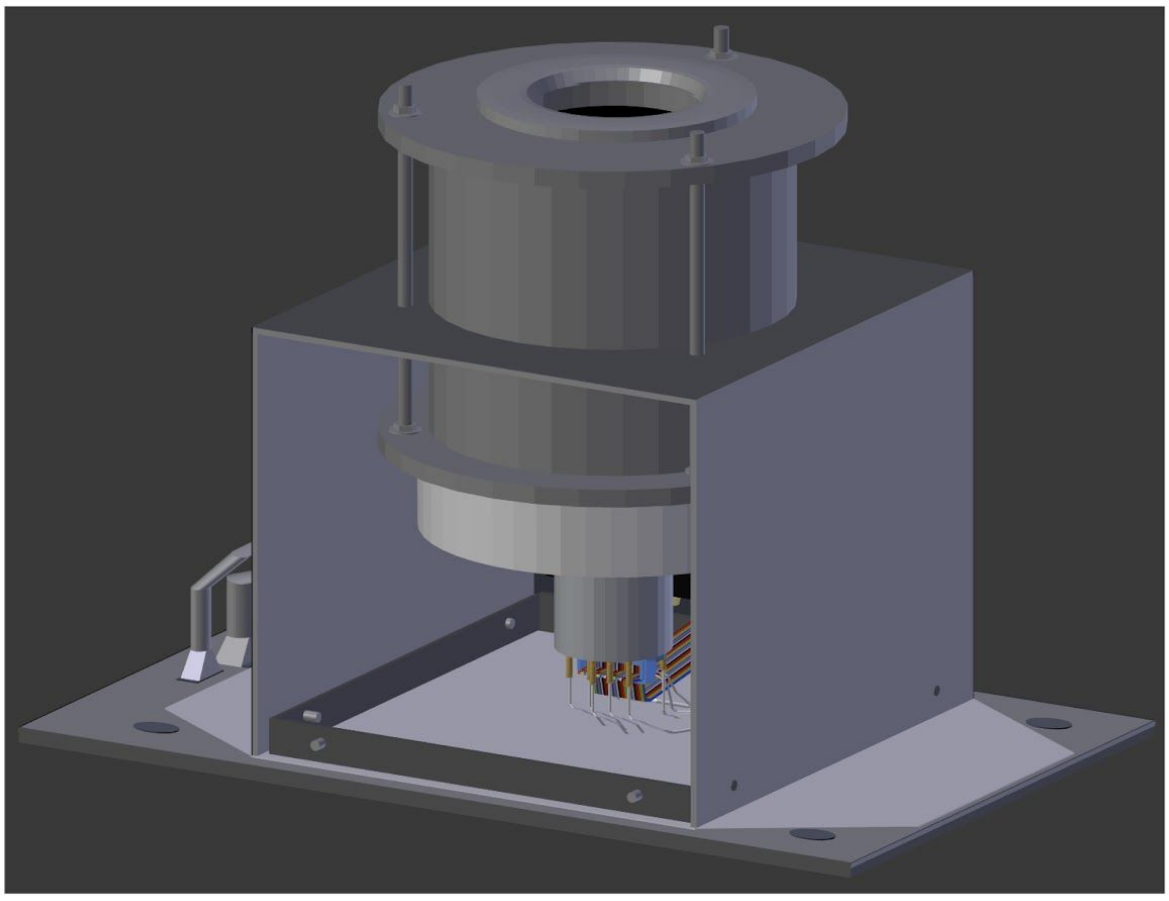

Fig. 25 - The SSGX mechanical model is shown here.

4.2 Power Circuit Diagrams

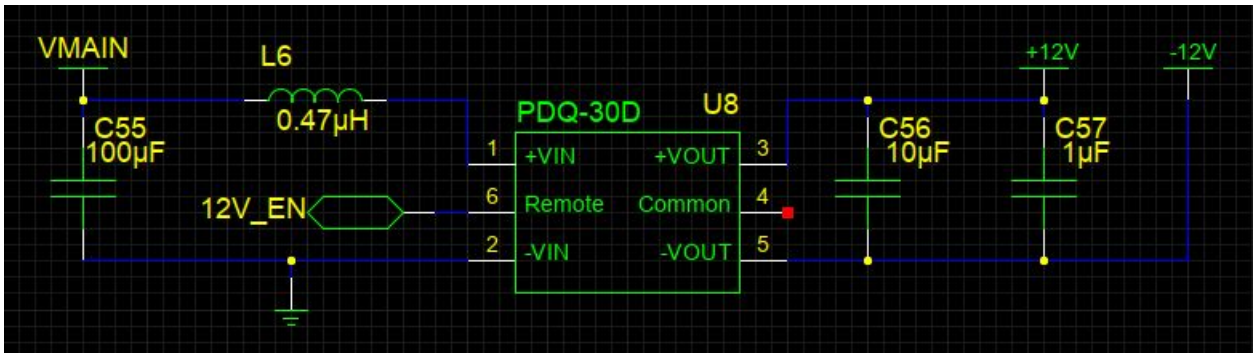

Fig. 26 - Schematic diagram for regulator: +/- 12 V (CdTe detector).

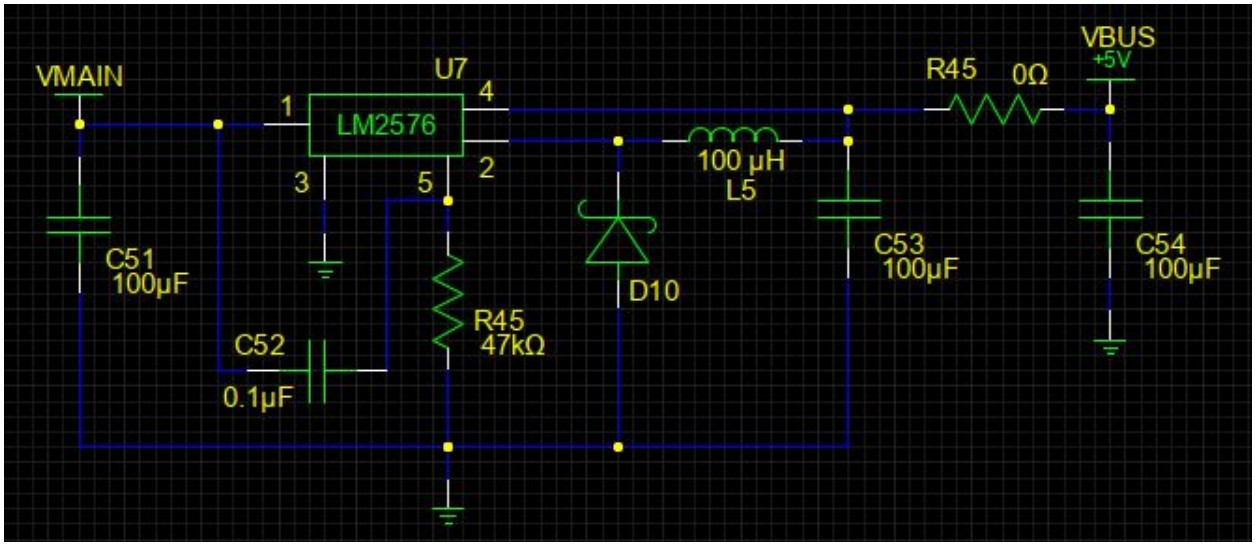

Fig. 27 - Schematic diagram for regulator: +5 V (Main).

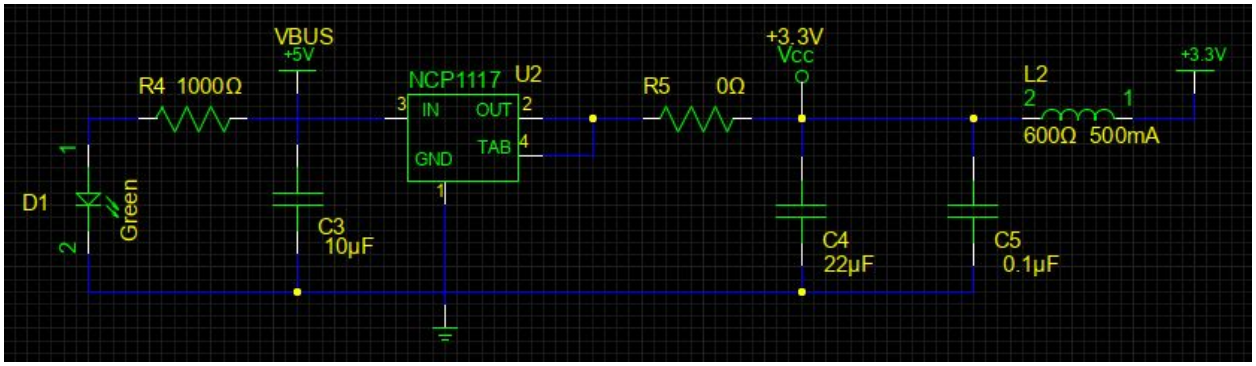

Fig. 28 - Schematic diagram for regulator: +3.3 V (Main).

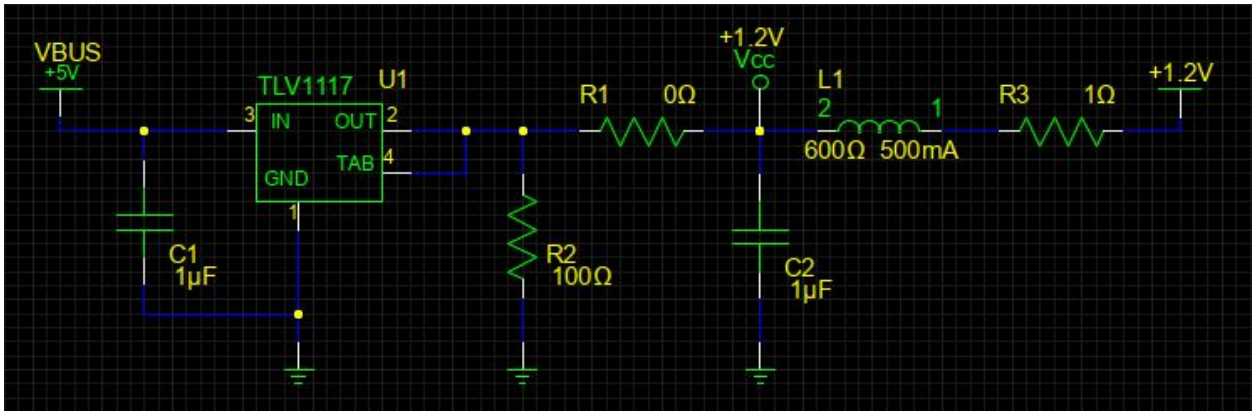

Fig. 29 - Schematic diagram for regulator: +1.2 V (CPLD).

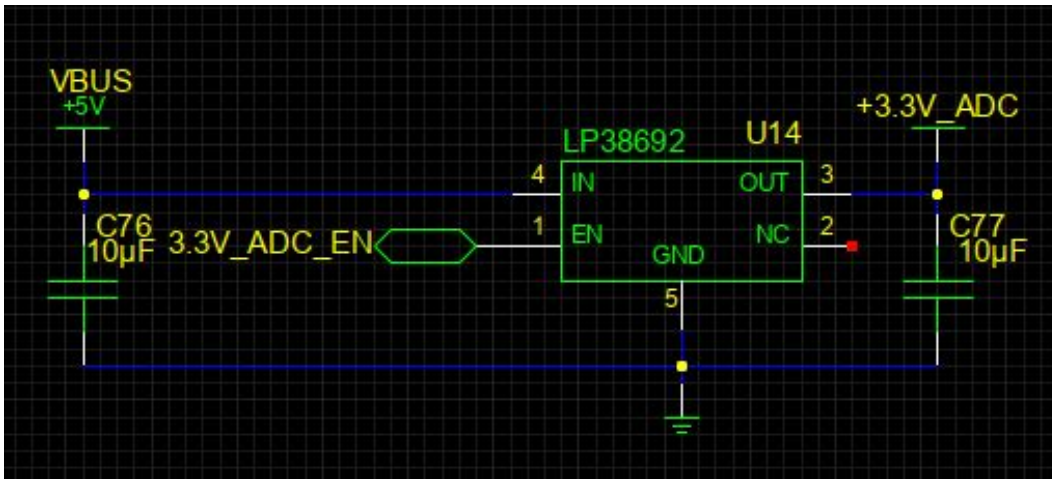

Fig. 30 - Schematic diagram for regulator: +3.3 V (ADC).

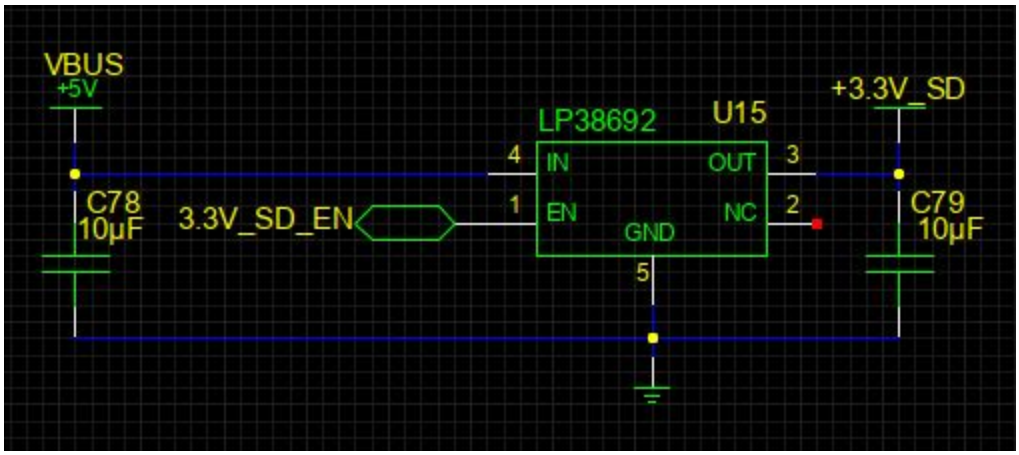

Fig. 31 - Schematic diagram for regulator: +3.3 V (SD).

4.3 Additional Schematic Diagrams

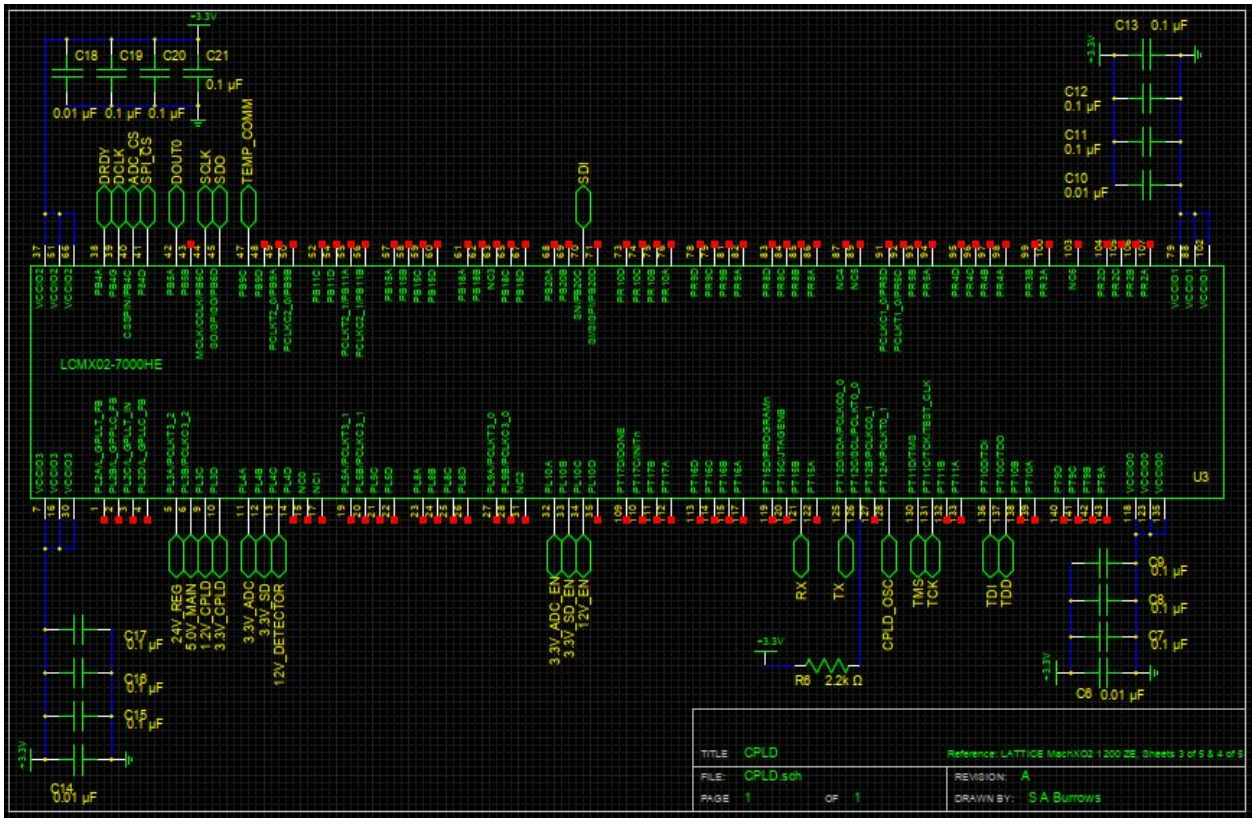

Fig. 32 - Schematic diagram for the CPLD.

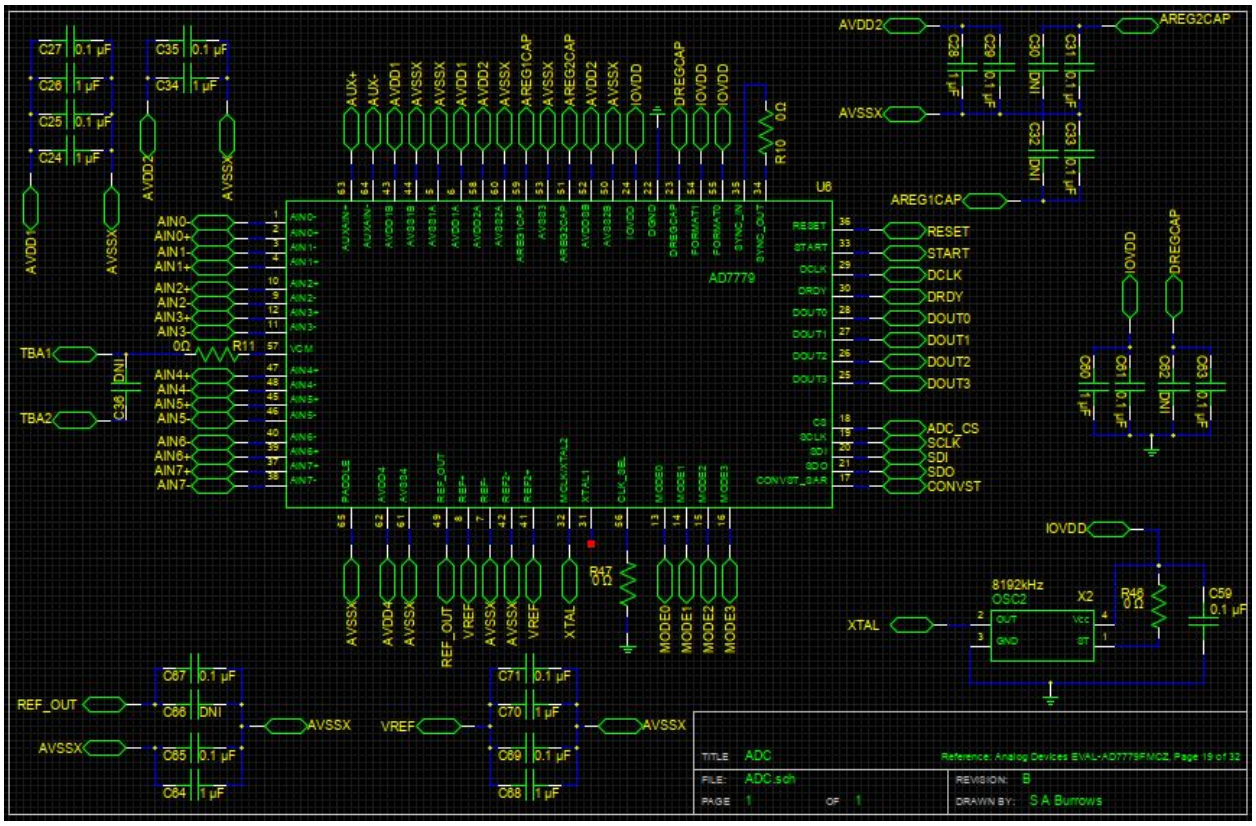

Fig. 33 - Schematic diagram for the ADC circuit, with oscillator.

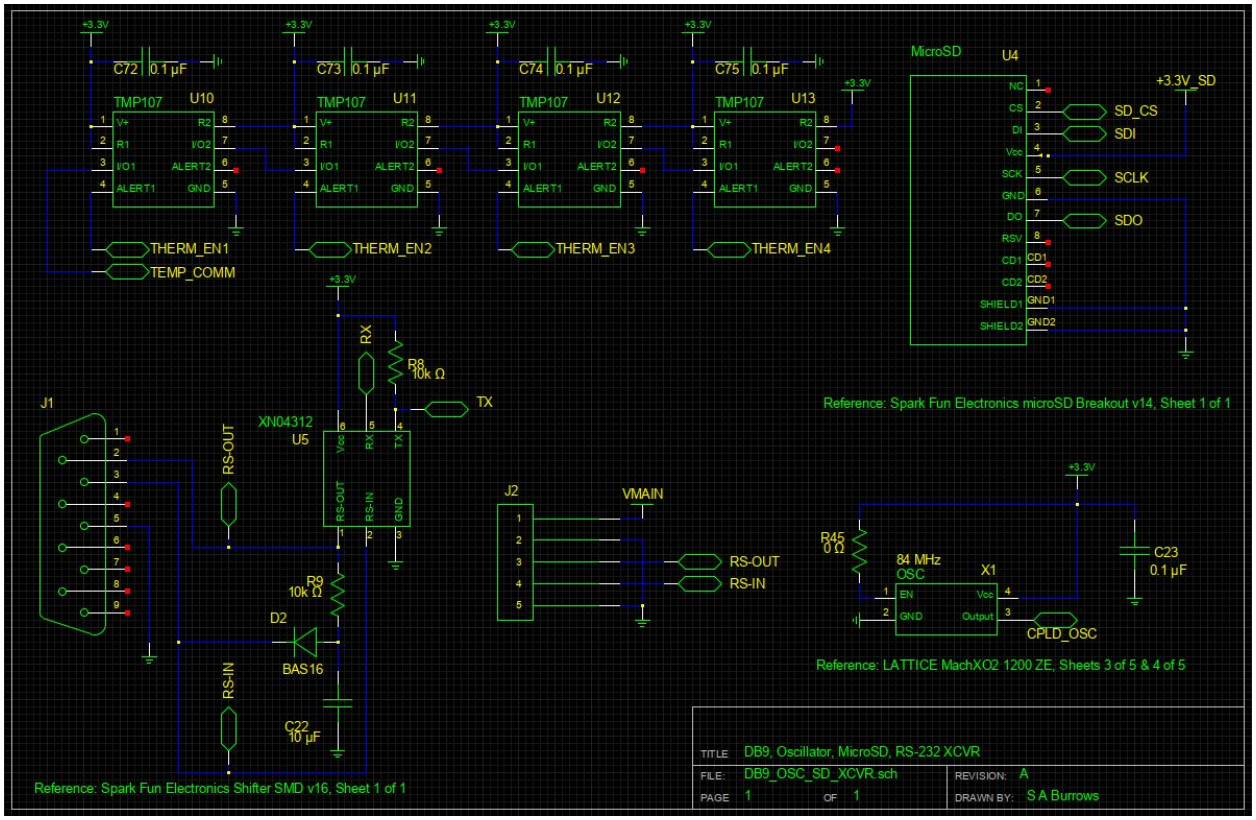

Fig. 34 - Circuits for temperature sensors, CPLD oscillator, RS-232, and SD card.

References

[1] A. J. Dean, et al, “Polarized gamma ray emission from the CRAB”, Science, vol. 321, no 5893, p. 1183, 2008.
[2] R. Novick, M.C. Weisskopf, R. Berthelsdorf, et al., “Detection of X-Ray Polarization of the Crab Nebula”, Ap.J., 174, L1 (1972).
[3] M. C. Weisskopf, et al., “A precision measurement of the X-ray polarization of the Crab Nebula without pulsar contamination”, Astrophys. J. 220, L117 (1978).
[4] E. Suarez-Garcia, W. Hajdas, “POLAR: Design of a novel X-ray polarimeter based on plastic scintillators and MAPMTs”, Nucl. Instr. and Meth. A, 610, p. 276-279, 2009
[5] H. Krawczynski, A. Garson III, J. Martin, et al., “The Hard X-ray Polarization Sensitivity of the Energetic X-ray Imaging Survey Telescope EXIST”, PoS(CRAB2008)026.
[6] J. E. Hill, M. L. McConnell, P. Bloser, et al., “POET: POlarimeters for Energetic Transients”, AIP Conf. Proc., 1065, 331, 2008.
[7] J. Greiner, A. Iyudin, G. Kanbach, “Gamma-ray burst investigation via polarimetry and spectroscopy (GRIPS)”, Exp. Astr., 23, 91-120, 2009.
[8] C. Winkler, T.J. Courvosier, et al “The Integral Mission” Astron. Astr. 411, L1-L6 (2003)
[9] P. Ubertini, F. Lebrun, G. Di Cocco, et al., " IBIS: The Imager on-board INTEGRAL" Astronomy and Astrophysics, Vol 411, n. 1, p. L131, 2003.
[10] A. J. Dean, et al, “Polarized gamma ray emission from the CRAB”, Science, vol. 321, no 5893, p. 1183, 2008.
[11] M. Forot, et al., “Polarization of the Crab Pulsar and Nebula as Observed by the INTEGRAL/IBIS Telescope”, Ap.J., 688, L29, 2008.
[12] P. Laurent, J. Rodriguez, J. Wilms et al., “ Polarized Gamma-Ray Emission from the Galactic Black Hole Cygnus X-1”, Science, vol. 332 no. 6028 p. 438-439
[13] e-ASTROGAM mission white book draft 1
http://www.iaps.inaf.it/eastrogam/Doc/WB_e-ASTROGAM.pdf
[14] R. M. Curado da Silva, E. Caroli, J. B. Stephen and P. Siffert, “CIPHER, a polarimeter telescope concept for Hard X-ray Astronomy”, Exp. Astron., Vol. 15, nº1, p. 45-65, 2003.
[15] E. Caroli, R. M. Curado da Silva, A. Pisa, “Polarisation measurements with a CdTe pixel array detector for Laue hard X-ray focusing telescopes”, Exp. Astron. vol 20, p. 353-364, 2006.
[16] R.M. Curado da Silva, et al., “Polarimetric performance of a Laue lens gamma-ray CdZnTe focal plane prototype”, J. Appl. Phys., 104, p. 084903 (2008).
[17] Ezio Caroli, Rui M. Curado da Silva, John B. Stephen et al., “A Polarimetric Experiment With a Laue Lens and CZT Pixel Detector”, IEEE Trans. Nucl. Sci., Vol. 56, Nº 4, p. 1848-1854, 2009.
[18] R. M. Curado da Silva, N. Auricchio, E. Caroli, et al., “Polarimetry study with a CdZnTe focal plane detector”, IEEE Trans. Nucl. Sci., Vol. 58, 4, p. 2118-2123, 2011.
[19] R. M. Curado da Silva, E. Caroli, J. B. Stephen, “Polarization degree and direction angle effects on a CdZnTe focal plane performance”, IEEE Trans. Nucl. Sci., in press, 2012.
[20] E. Caroli et al., “A small 3D CZT payload for hard X-ray polarimetry and spectroscopic imaging”, Nuclear Science Symposium and Medical Imaging Conference (NSS/MIC), 2014 IEEE
[21] S. Antier et al.,“Hard X-ray polarimetry with Caliste, a high performance CdTe based imaging spectrometer”, Experimental Astronomy, March 2015

[22] E. Caroli et al., “CACTµS: A small CdTe array for a prototype balloon experiment”, Nuclear Instruments and Methods in Physics Research A 513 (2003) 357–361